

Scripta Materialia

High-Resolution 3D Strain and Orientation Mapping within a Grain of a Directed Energy Deposition Laser Additively Manufactured Superalloy --Manuscript Draft--

Manuscript Number:	SMM-23-0316R1
Article Type:	Regular article
Keywords:	Directed Energy Deposition, Laser Additive Manufacturing, Dark Field X-ray Microscopy, Electron Backscatter Diffraction, Microstructure
Corresponding Author:	Can Yildirim ESRF GRENOBLE, FRANCE
First Author:	Yunhui Chen
Order of Authors:	Yunhui Chen Yuanbo T Tang David M Collins Samuel J Clark Wolfgang Ludwig Raquel Rodriguez-Lamas Carsten Detlefs Roger R Reed Peter D Lee Philip J Withers Can Yildirim
Abstract:	<p>The industrialization of Laser Additive Manufacturing (LAM) is challenged by the undesirable microstructures and high residual stresses originating from the fast and complex solidification process. Non-destructive assessment of the mechanical performance controlling deformation patterning is therefore critical. Here, we use Dark Field X-ray Microscopy (DFXM) to map the 3D subsurface intragranular orientation and strain variations throughout a surface-breaking grain within a directed energy deposition nickel superalloy. DFXM results reveal a highly heterogenous 3D microstructure in terms of the local orientation and lattice strain. The grain comprises $\approx 5 \mu\text{m}$-sized cells with alternating strain states, as high as 5×10^{-3}, and orientation differences $< 0.5^\circ$. The DFXM results are compared to Electron Backscatter Diffraction measurements of the same grain from its cut-off surface. We discuss the microstructure developments during LAM, rationalising the development of the deformation patterning from the extreme thermal gradients during processing and the susceptibility for solute segregation.</p>

European Synchrotron Radiation Facility
71 Avenue des Martyrs, CS40220, 38043 Grenoble Cedex 9, France
Phone: +33 (0)4 38 88 27 62

Dear Editor,

Please find attached our submission entitled “High Resolution 3D Strain and Orientation Mapping within a Grain of a Directed Energy Deposition Laser Additively Manufactured Superalloy” to be considered for publication in Scripta Materialia.

In this work, we present novel insights the investigation of the microstructure at grain level produced by Directed Energy Deposition Additive Manufacturing (DED-AM) utilising Synchrotron X-ray Dark Field Microscopy (DFXM) in combination with Diffraction Contrast Tomography (DCT) and Electron Backscatter Diffraction (EBSD).

For the first time, we demonstrate a unique non-destructive mapping of the 3D intragranular orientation and strain variations of a Laser Additive Manufacturing (LAM)-formed grain from its surface into the bulk with highest angular resolution possible using DFXM. The DFXM results reveal a highly-heterogenous and complex 3D microstructure in terms of the local orientation and lattice strain. We show that the LAM-formed grain in the as-fabricated state has residual stresses that almost reach the yield strength of the material, which should be considered for subsequent heat treatment processes for the material. The DFXM results of the grain of interest were compared with EBSD measurements of the same grain, from its free surface. We believe that our contribution brings a new perspective and a detailed description of the intricate physics at play during LAM, including rapid solidification and solute segregation, hence will be of key interest to Scripta Materialia readers.

We believe that this study will provide an invaluable ground truth for experiments and computational model validation. Such advancements are critical for new alloy and process design. The novel DFXM analysis methodology that has been adopted in this study will significantly contribute to a much wider field of research. This includes increasing the quantitative detail that cannot be obtained from current techniques for LAM.

Should you select our manuscript for peer review, we would like to suggest the following potential reviewers/referees because they would have the requisite background to evaluate our findings and interpretation objectively:

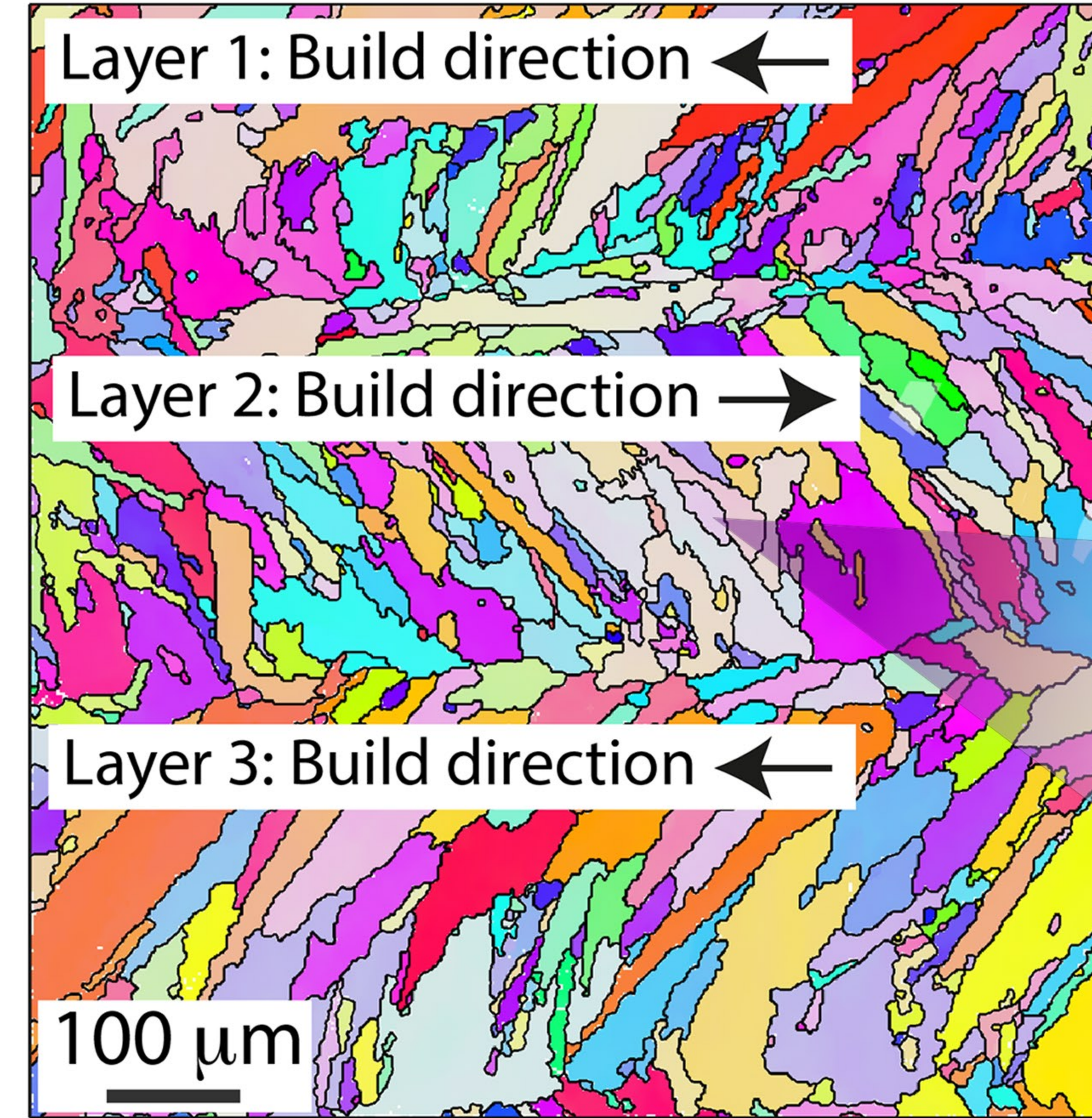
- Tresa Pollock, UC Santa Barbara, pollock@engineering.ucsb.edu, an expert in additive manufacturing of structural materials and their characterisation
- Jochen Kittel, Fraunhofer Institute for Laser Technology, jochen.kittel@ilt.fraunhofer.de, an expert in additive manufacturing, especially DED-AM
- Constantinos Goulas, University of Twente, k.goulas@utwente.nl, an expert in additive manufacturing and physical metallurgy

We confirm that this work is original and has not been published elsewhere, nor is it currently under consideration for publication elsewhere. We have no conflicts of interest to disclose. Thank you for your consideration of this manuscript in your reputable journal. We are looking forward to your editorial decision.

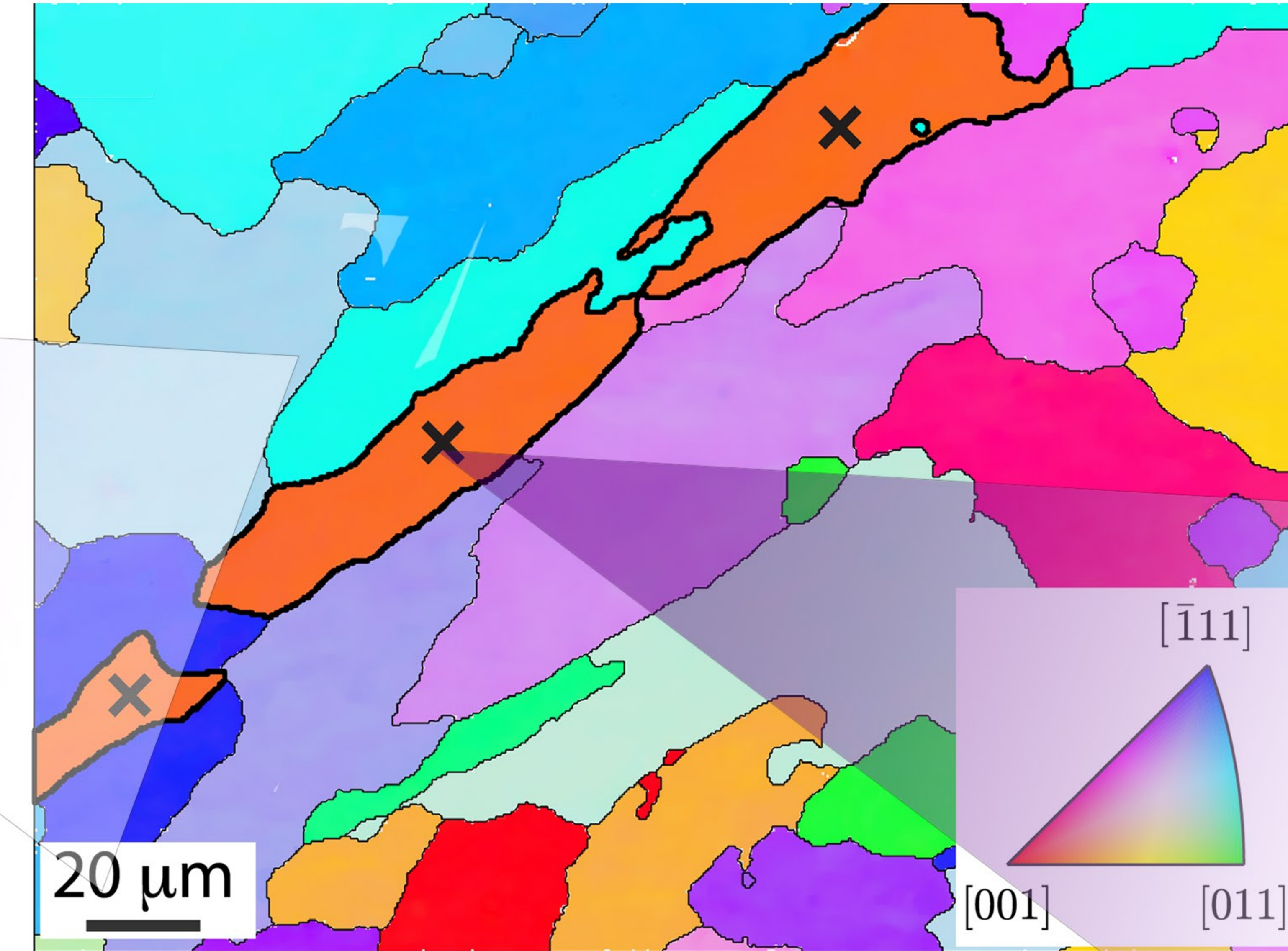
With kind regards,

C. Yildirim and Y. Chen on behalf of all authors

High Resolution 3D Strain and Orientation Mapping within a Grain of a Directed Energy Deposition Laser Additively Manufactured Superalloy

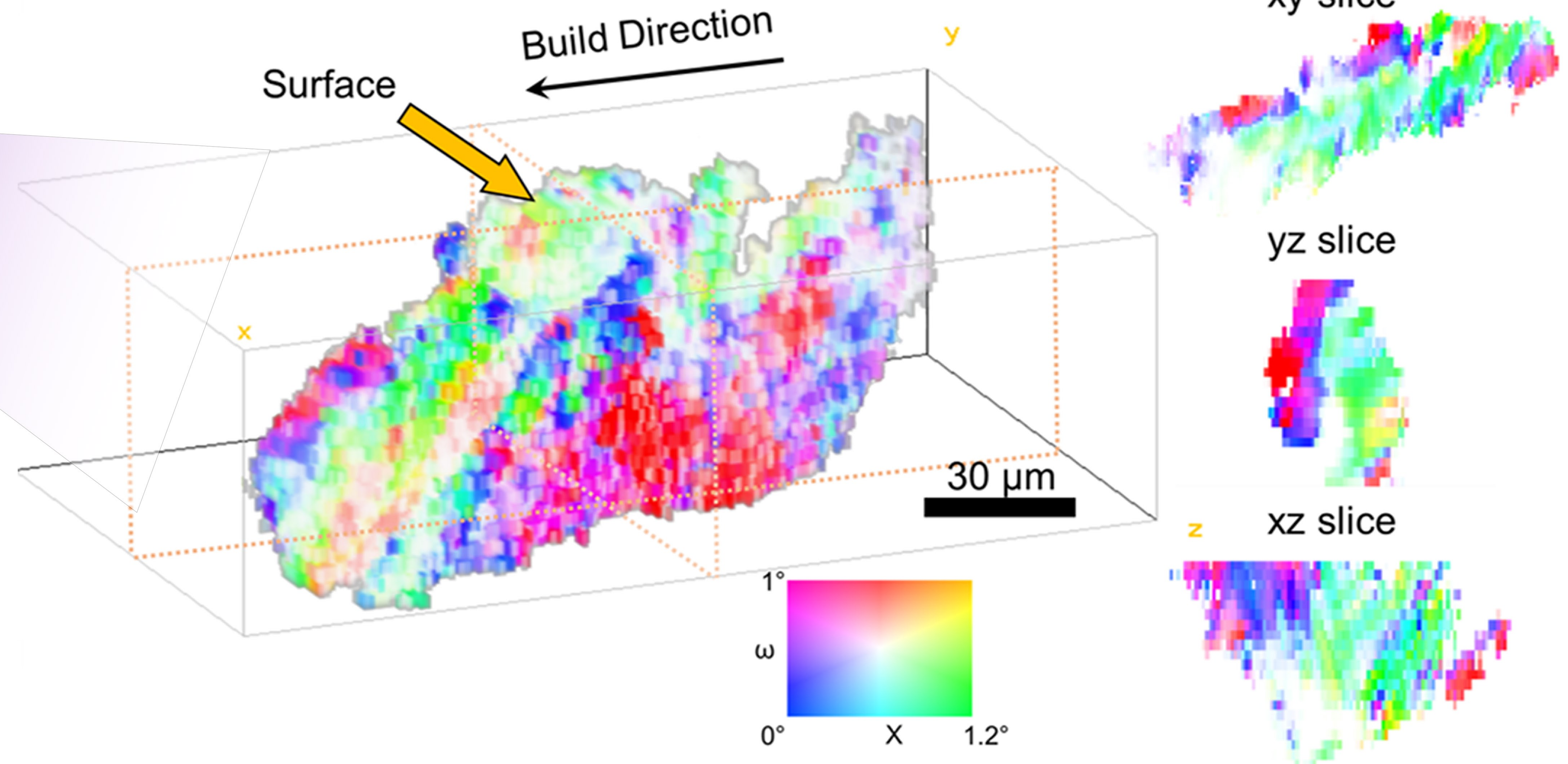


Complex microstructures are formed in laser additive manufacturing due to rapid solidification.



Residual stresses and orientation variations significantly affects the mechanical properties.

Dark Field X-Ray Microscopy reveals the inhomogeneous 3D distribution of local strain and orientation of LAM-formed grain.



RESPONSE LETTER AND THE LIST OF CHANGES IN THE REVISE MANUSCRIPT SMM-23-0316

This is the 1st revision of the manuscript entitled “High Resolution 3D Strain and Orientation Mapping within a Grain of a Directed Energy Deposition Laser Additively Manufactured Superalloy”. The authors are grateful to the reviewers for their critical appraisal of the manuscript, and we sincerely appreciate, not only the comments themselves, but the requisite time spent to review our work. Their efforts are highly appreciated. Reviewers’ suggestions were adopted and are marked in blue color in the newly submitted manuscript text. Below, we explain how we handled the reviewers’ comments point by point in blue.

Reviewer #1:

The authors present a heroic effort combining DFXM and HR-EBSD to characterize lattice orientation and strain distributions within a nickel superalloy grain in a specimen manufactured with DED. The manuscript is worthy of publication, but a few comments / concerns should be addressed.

* I don't think I would describe these measurements as non-destructive as implied in the abstract (nor am I sure DFXM will ever be for AM components). Maybe 3D or subsurface?

We changed the wording to subsurface. We note that e.g. thermal treatment could still be performed on the sample for a before-after (or possibly in-situ) study. Our work in this direction is on-going.

* While I understand what the authors are trying to do, you just can't multiply the lattice strain by the directional modulus in this situation to calculate a stress. The 111 normal is almost aligned to the surface normal (if I'm reading 2a correctly), and as you are still pretty close to the surface, I would expect the stress to be pretty close to biaxial so the 111 strain reflects Poisson expansion/contraction. Regardless, I don't think the stress comments add anything to the science and are likely incorrect. Remove the stress from both the manuscript and supplement or find a way to do a more accurate analysis.

Given that our main points are to determine the deformation patterning features, we feel this is sufficiently well described by the presented strains. We are thus happy to remove the stresses as they are not needed to underpin the conclusions made by this work.

* I'm surprised the lattice strain fields don't seem to also reflect the cell structure implied from the misorientation. Please comment.

In DFXM strain maps, we show the measured elastic strains using the variation of the d spacing on 111 planes. This is achieved by measuring a single Bragg reflection, we probe variations of the lattice parameter in the 2θ direction, i.e. axial strain $\delta d/d$ along that particular direction. In

the “mosaicity scan” using which the misorientation maps are generated, the scattering angle 2θ is kept fixed, and we measure tilts of the Bragg planes. They can correspond to a rotation of the unit cell, shear strains, or a combination thereof. Thus, if the d spacing changes within a given crystal due to strain gradients, imaging at a single 2θ point will not provide the full information of the crystal. Indeed, the best way to deal with this issue is to have scans that cover the entire 3D orientation space (ϕ , χ , 2θ). However, these scans are highly time consuming compared to 2D scans of the orientation space while having a representative number of 2D layers in the volume.

* Since the HR-EBSD has all six strain components measured, you should be able to project the ebsd strains along the 111 / q direction for 1-to-1 comparison with the DFXM at the surface. This would be much more illuminating than 5b.

The authors agree this was a good idea and have now replaced Figure 5b with the projected 111 strains from the EBSD data. In this new orientation, it is evident that a band of tensile strain runs along the length of the grain, replicating the DXFM observation. As this feature was not observable before, it was satisfying to see this new collaboration between the techniques. The narrative in the body text has been updated accordingly. The full strain tensor from the EBSD has now been moved to the Supplementary Material for completeness.

* Pg 3 Line 24, I think this is a typo referring to $200 \times 200 \text{ mm}^2$.

We corrected it, thank you for spotting.

Reviewer #2:

The paper present some interesting results with regard to characterization of microstructure and internal strain of a superalloy manufactured by a additive manufacturing process. In particular the work demonstrates the extent and type of information available from examination using the dark-field X-ray microscopy technique, allowing measurements to be made in the interior (below the surface) of a sample. The presented results provide some novel information regarding the nature of the microstructure and strain and are discussed with regard to previously collected data based only of 2D (surface) measurements. The work is in general well presented though in some places some additional information, or a clearer description, will be helpful, and in other places it is suggested the authors are more cautious in their statements regarding the novelty of the obtained results.

1. It was not clear to the reviewer what a "bi-directional thin wall sample" actually means - and indeed if this is even relevant, when their characterization is focused only one part of this sample (so the overall shape seems to be irrelevant for this study). Do they just mean the sample is in effect a vertically-standing thin plate?

Yes. We changed the wording to “vertically-standing thin plate”.

2. Following from above, either in the figure or in the caption, it will help to confirm the relationship between Fig. 1a and Fig. 1b (I assume this is the same viewing plane). Also do not use "IPF-Z" as a description as this is meaningless unless we are told what direction "Z" corresponds to.

We modified the caption for clarity.

3. Can the authors somehow make clear how the imaged volume using DFXM (e.g. as shown in Fig. 2b) relates to the "grain" under investigation (shown in Fig. 1c and 1d as marked with "X"s). For, example is the imaged volume just the central part of this grain? Why does the surface layer (Fig. 2c) not match the appearance at the surface of the grains as seen in the EBSD map (Fig. 2e). I imagine that I have simply misunderstood the geometric relationship between the different areas - but if that is the case then some help for other readers to avoid the same confusion will benefit the work.

DFXM measures the projection of a grain from a specific crystallographic plane (e.g., 111) using an angular offset determined by the Bragg angle. Additionally, the use of a line-focused beam in DFXM introduces an asymmetric aspect ratio, scaled by $1/\sin 2\theta$, in one direction. In contrast, EBSD scans each point on the surface independently. While the longitudinal length of the grain remains the same in both DFXM and EBSD, the asymmetry arises from the geometric effect caused by the incoming beam and the theta angle offset on the 111 projection.

We modified the Figure 2 caption as follows:

"In (b) and (e), the grain size in the elongated direction is equivalent. However, an asymmetric aspect ratio arises from the incoming line-focused beam in DFXM, with a factor of $1/\sin(2\theta)$. The CRLs filter out the invisible parts in (c) and (d) due to high lattice curvature and/or lattice strain in those areas."

4. The authors should consider a different name for describing Fig. 2c. The term "misorientation map" will be understood by many as showing voxel-to-voxel misorientations, whereas in fact this is "deviation to average" type plot (maybe a "reference misorientation map"?)

We changed the wording as "map showing the angular deviation from the grain's average orientation" in the figure caption:

"Note that the misorientation map shows the angular deviation from the grain's average orientation."

5. (page 4; column 2; lines 5-8). My understanding of the structure in this SLM-printed alloy is that the cell structure, at a scale of 750 nm cells, is present throughout the microstructure. In the present work features that may correspond to these cells are seen, but only in some places. As

such this is more a demonstration of a limitation of this method to fully reveal the microstructure, is worthy of note as such.

Our DFXM results show two types of cell structure in this grain. The first one is the larger cells having ~5-7 micron sizes consistent with the previous studies (Tang et al, Additive Manufacturing, 2023) on this alloy. The second cell structure is at a smaller scale, and visible only in some places as the reviewer pointed out. The current spatial resolution of the DFXM technique is ~120-150 nm, however thanks to the high angular resolution of DFXM, we can see subtle local lattice rotations and strain even though the feature sizes may be at close to the limits of the instrument. Also note that, we define these cells based on the misorientation levels, indicative of the higher dislocation density compared to the surrounding matrix.

6. (page 4; column 2; lines 44-52) I suggest the authors rethink the interpretation of this text. They claim that the results support a high density of GNDs. The GND density though is calculated based on lattice curvature - and a high GND density implies a high lattice curvature - but if that were the case then such a high-angular resolution technique such as DFXM (or cross-correlation) would not be needed (so they comments here are arguing against the novelty of this work ...). In fact the misorientation angles across the cell walls are very low (so that can only be imaged using a high-angular resolution method) - and so by the conventional definition of "GNDs" the density must also be low. In fact the dislocation density in cell boundary walls in SLM-printed metals is very high - but these are not geometrically necessary (in the usually discussed sense).

We thank the reviewer for bringing this up. What we meant by high dislocation density is higher than the surrounding matrix, so that we can see an increase of the misorientation based on the lattice curvature. We modified the text accordingly.

Also note that there is an underestimate due to only a limited amount of the lattice curvature being measured in DFXM, and hence its magnitude is underestimated and so is the GND density. Similarly, EBSD does not measure the full rotation field (as it's just surface components), so is similarly a lower bound estimate. We modified the GND as GND₁₁₁ in the text for clarity.

7. (page 5; column 2; line 23). The authors are advised to make clear exactly what "strain spread" means (maximum difference in absolute values - or maybe some measure of the distribution width?)

Similar to our recent papers (Mavrikakis, et al, Acta Mat. 2019, Bucsek et al. Acta Mat. 2019), the reference points for a scan were chosen as the highest intensity point at a given Bragg reflection. In this study we performed the same method for consistency with our previously published data. Note that the alignment procedure includes the

optimization of a Bragg peak intensity of a given reflection on the farfield firstly without the X-ray objective objective, and then a finer optimization with the objective. The reference 2θ value is then determined as the highest intensity point, which is taken as the nominal value around which a scan is performed. Thus, we show the strain gradients within the grain around the local $d0$ value. The term “strain spread” indicates the width of the strain distribution around this $d0$ value. We have modified the figure caption accordingly.

8. The authors may wish to consider showing only one strain component in Fig. 5b, as at present, even using the high-resolution image provided it is very difficult to see the detail regarding the similarity in appearance with Fig. 8a, as claimed by the authors (perhaps including the other strain component maps in a larger size as a supplementary figure).

We replaced fig 5b with the 111 projection of the EBSD strain measurements and moved the first version of fig 5b to the supplementary material.

9. (page 6; column 1; lines 44-46). In their summary the authors should consider being more specific in stating the advantage of DFXM method. At present they write that surface based techniques "... provide data that is not representative ...". I certainly agree that with regard to the strain measurements and some aspects of the orientation variation this is true. It is ironic though that they interpret the weakly-detected striped features in Fig. 3c as being the cells, with Ti segregation observed in TEM samples ... (the extreme case of a surface measurement) - clearly showing that not all aspects of surface based measurements are "not representative". A little more caution in the language in describing the specific advantages of their method will help.

We agree with the referee. We changed that sentence as follows:

“This demonstrates that DFXM provides representative bulk information of complex subsurface microplasticity for materials fabricated via LAM.”

High-Resolution 3D Strain and Orientation Mapping within a Grain of a Directed Energy Deposition Laser Additively Manufactured Superalloy

Y. Chen^{a,b,c,g}, Y.T. Tang^d, D.M. Collins^e, S.J. Clark^f, W. Ludwig^b, R. Rodriguez-Lamas^b, C. Detlefs^b, R.C. Reed^d, P.D. Lee^c, P.J. Withers^g, C. Yildirim^{b,*}

^a*School of Engineering, RMIT University, Melbourne, 3000, Australia*

^b*European Synchrotron Radiation Facility, 71 Avenue des Martyrs, CS40220, 38043 Grenoble Cedex 9, France.*

^c*Mechanical Engineering, University College London, Torrington Place, London WC1E 7JE, UK*

^d*Department of Materials, University of Oxford, Oxfordshire, UK*

^e*School of Metallurgy and Materials, University of Birmingham, Edgbaston, Birmingham B15 2TT, UK*

^f*X-ray Science Division, Advanced Photon Source, Argonne National Laboratory, Lemont, IL 60439*

^g*Henry Royce Institute, Department of Materials, University of Manchester, Oxford Road, Manchester, UK*

Abstract

The industrialization of Laser Additive Manufacturing (LAM) is challenged by the undesirable microstructures and high residual stresses originating from the fast and complex solidification process. Non-destructive assessment of the mechanical performance controlling deformation patterning is therefore critical. Here, we use Dark Field X-ray Microscopy (DFXM) to map the 3D subsurface intragranular orientation and strain variations throughout a surface-breaking grain within a directed energy deposition nickel superalloy. DFXM results reveal a highly heterogeneous 3D microstructure in terms of the local orientation and lattice strain. The grain comprises $\approx 5 \mu\text{m}$ -sized cells with alternating strain states, as high as 5×10^{-3} , and orientation differences $< 0.5^\circ$. The DFXM results are compared to Electron Backscatter Diffraction measurements of the same grain from its cut-off surface. We discuss the microstructure developments during LAM, rationalising the development of the deformation patterning from the extreme thermal gradients during processing and the susceptibility for solute segregation.

Keywords:

Directed Energy Deposition, Laser Additive Manufacturing, Dark Field X-ray Microscopy, Electron Backscatter Diffraction, Microstructure

Laser Additive Manufacturing (LAM) is a powerful and versatile technique for the direct layer-by-layer fabrication of complex 3D components from metallic alloy powders/wires [1] having the potential to revolutionize manufacturing processes. LAM is driven by component requirements such as unconventional geometries, small production numbers, digital manufacturing, and high-value-added applications in aerospace, power generation, and biomedical industries. Directed Energy Deposition LAM (DED-LAM) is amongst the most promising methods in LAM for industrial applications, allowing for building large freeform components and also offering *in-situ* repairability. However, technological challenges restrict the mechanical performance of final products fabricated via LAM. The material experiences rapid cooling at $\approx 10^4 - 10^6 \text{ K/s}$, ca. $10^5 \times$ faster than conventional processes (ca. $1-10 \text{ K/s}$) [2]. The high cooling rate associated with laser processing can result in microstructural defects, introducing significant levels of residual stresses and high dislocation densities in the as-fabricated state. Highly-localized melting and non-

equilibrium solidification dynamics create residual stresses on the order of $> 600 \text{ MPa}$ in 316L stainless steel [3, 4]. These stresses have a detrimental effect on the mechanical performance of the products, causing defects including cracking, delamination, and loss of dimensional accuracy. Therefore, understanding the stress state of these complex microstructures is of significant technological importance.

A commonly-used technique for the characterization of AM microstructures is Electron Backscatter Diffraction (EBSD), which can quantify information about the structure [5], crystal orientation [6], phase [7] or strain [8] in the material. The measured diffraction signal typically comes from the surface $10-50 \text{ nm}$ of the sample. Combined with focused ion beam (FIB) layer-by-layer sectioning, it is possible to obtain 3D information on the microstructure. However, destructive specimen preparation (i.e. sectioning and polishing) may alter the microstructure near the surface and precludes dynamic studies in 3D. These methods inevitably suffer from surface relaxation of residual stresses, making it impossible to interpret the bulk behavior of the stress distribution. The influence of such surface effects is difficult to quantify, making microstructure assessments with high confidence difficult.

*Corresponding Author

Email address: can.yildirim@esrf.fr (C. Yildirim)

Among non-destructive methods, synchrotron X-ray imaging has proved a powerful technique, capturing features such as porosity and regions where the powder was not fused in mm-sized samples. The technique allows for dynamic studies thanks to high image acquisition rates [9, 10, 11]. Using X-ray micro-computed tomography (μ CT), non-destructive volumetric characterization of additively-manufactured parts can be achieved [12, 13]. While these methods provide important insights, they do not provide information on the strain or crystal orientations of the material. Over the last 20 years, diffraction-based synchrotron imaging techniques such as 3D X-ray Diffraction (3DXRD)/High Energy Diffraction Microscope (HEDM)[14] and Diffraction Contrast Tomography (DCT)[15] have been used extensively to map grain structures in 3D. Although these techniques provide grain-level orientation and strain in a given volume, they provide limited information on the intragranular level due to their spatial resolution ($\approx 1 - 2 \mu\text{m}$). Moreover, the strain and orientation spreads that are caused by the high cooling rates make 3D reconstruction difficult (due to diffraction peak-overlap problems in indexing). Non-destructive characterization of the strain and orientation state of the intragranular cellular microstructure of rapidly-cooled AM parts thereby remains a challenge.

Dark Field X-ray Microscopy (DFXM), an emerging synchrotron imaging technique, can address the above-mentioned challenges. DFXM is a powerful diffraction-based technique for imaging strains and orientations in mm-sized crystalline materials with $\approx 150 \text{ nm}$ spatial and 0.001° angular resolutions, respectively [16, 17]. Using an objective lens analogous to a dark field transmission electron microscope offers bulk sensitivity in probing the intragranular details for a grain of interest (GOI).

In this paper, we aim to unveil as-fabricated intragranular microstructures in a DED-LAM formed superalloy in order to build connections with the physicochemical aspects of rapid solidification during manufacturing. Using DFXM, we characterize the 3D orientation variation and strain distributions of grain from its cut-off surface to the fully embedded interior. We compare DFXM results with EBSD measurements of the *same* grain.

A **vertically-standing thin plate** sample of ABD-900AM nickel superalloy [18], manufactured using DED-LAM, was sectioned in the middle perpendicular to the build plane for EBSD analysis. The sample was prepared via an abrasive metallographic route, finishing with colloidal silica. Figure 1(a) shows the EBSD micrograph revealing an overview of the additively-manufactured columnar grains that follow the heat transfer direction. Distinctive grain morphology differences can be observed throughout each build layer. A cantilever (Figure 1(b)) was prepared from the top layer of the sample with the following procedures: Electro Discharge Machining (EDM) was firstly used to section the specimen into a slice of $11 \times 6 \times 0.3 \text{ mm}^3$ (w/h/t) along the orientation parallel to the build direction. The slice was then mechanically ground to $200 \mu\text{m}$

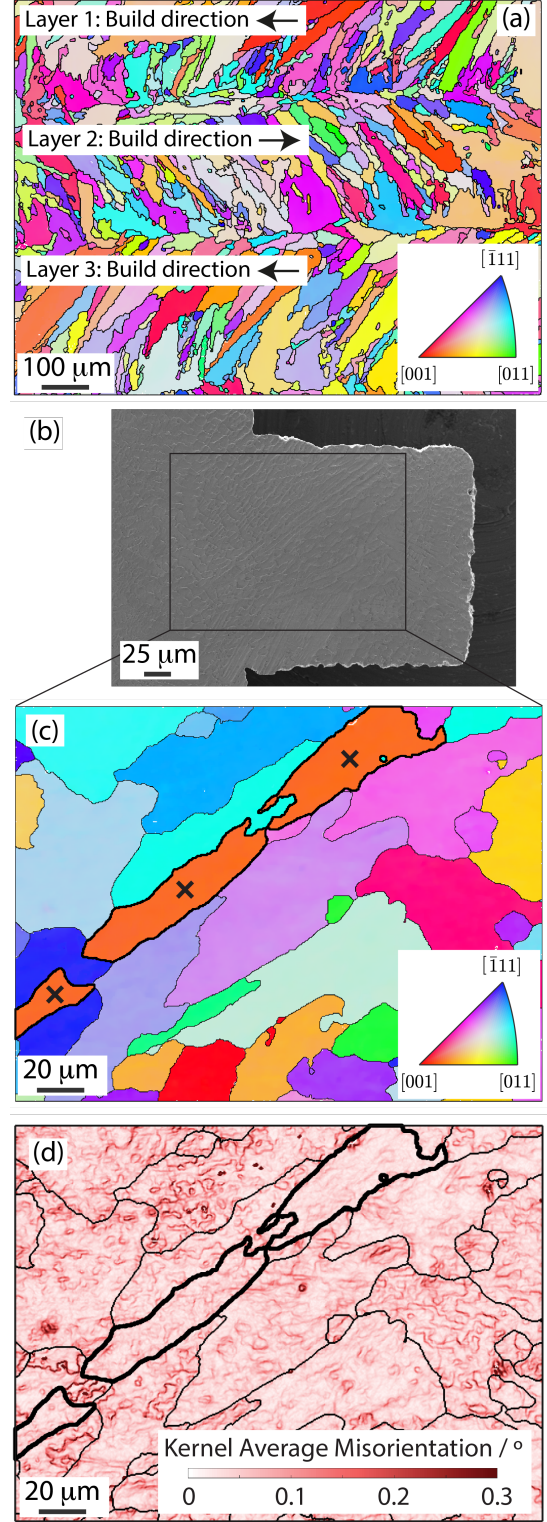


Figure 1: From a **vertically-standing thin plate** sample manufactured via DED-LAM: (a) an IPF-Z orientation map obtained using EBSD, where Z is the normal direction to the sample surface. An SE image of the sample examined by DFXM is shown (b) in this was taken from the Layer 2 region shown in (a), from which (c) an EBSD, IPF-Z map was obtained at high angular and spatial resolution, with 'x' denoting the surface breaking grain observed by DFXM. In (d) the Kernel Average Misorientation (KAM) map from the EBSD dataset is shown.

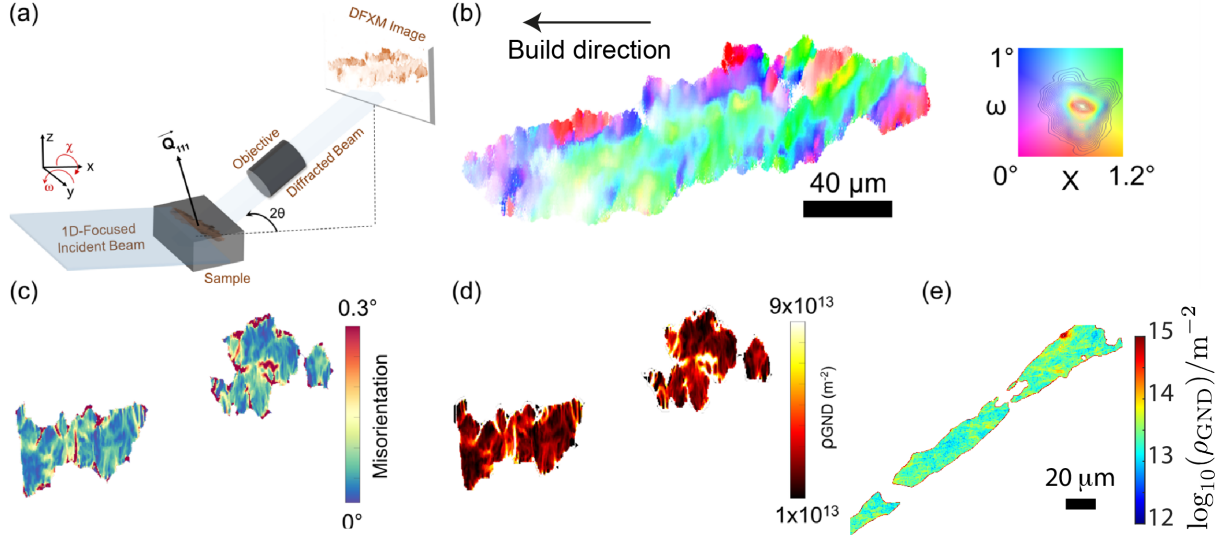


Figure 2: Synchrotron Dark Field X-ray Microscopy (DFXM) characterization of a Laser Additive manufactured grain. (a) Schematics of DFXM. (b) DFXM mosaicity map of a layer $30\ \mu\text{m}$ below the surface of the grain, with the inset showing the local 111 pole ($2\theta = 20.36^\circ$) figure color key of the two sample tilts (ω and χ). The mosaicity scans at the constant 2θ angle reveal the spatial variation of the orientation of the lattice around the 111 scattering vector. (c) DFXM misorientation map of the surface layer emphasizing the boundaries and cells (d) calculated GND density map. **Note that the misorientation map shows the angular deviation from the grain's average orientation.** The length scale in (b) applies to (c) and (d). (e) GND density map from the EBSD measurements. **In (b) and (e), the grain size in the elongated direction is equivalent. However, an asymmetric aspect ratio arises from the incoming line-focused beam in DFXM, with a factor of $1/\sin(2\theta)$.** The CRLs filter out the invisible parts in (c) and (d) due to high lattice curvature and/or lattice strain in those areas.

in thickness. Laser micromachining was then employed to section a foil of $2 \times 2.5\text{ mm}^2$ to form a square cantilever of $200\ \mu\text{m} \times 200\ \mu\text{m}$. Laser damage, if any, was subsequently removed by further electropolishing using 85 wt% phosphoric acid (H_3PO_4) in an aqueous solution with a DC voltage of 3 V for 60 s. Prior to the EBSD data collection, the material was ion polished using a Gatan PIP2 at 8 kV for 24 mins. The incident beam and the sample surface were positioned at 8° .

The sample was characterized by EBSD using a Zeiss Merlin field emission gun scanning electron microscope (FEG-SEM). Two magnifications were acquired for the cantilever, at a step size of $0.73\ \mu\text{m}$ & $0.45\ \mu\text{m}$. The higher resolution EBSD patterns (Figure 1(c)) were used to infer the geometrically necessary dislocation (GND) density and residual elastic strain maps using an in-house developed MATLAB code. Here, the diffraction patterns were analyzed using a cross-correlation-based method. More details about the HR-EBSD method and its mathematical basis be found elsewhere [19, 20, 21, 22].

The DFXM experiments were carried out at the beamline ID06-HXM at the European Synchrotron Facility [23]. An incident monochromatic beam with a photon energy of 17 keV was focused in the vertical direction onto the sample using a Compound Refractive Lens (CRL). The beam profile on the sample was $\approx 200 \times 0.6\ \mu\text{m}^2$ (FWHM) in the horizontal and vertical directions, respectively. The horizontal *line beam* illuminated a single plane that sliced through the depth of the crystal, defining the *observation plane* for the microscope. A detector comprising a scintillator crystal, a visible microscope, and a 2160×2560 pixel² PCO.edge sCMOS camera was located 5300 mm away from

the sample. This camera had exchangeable $10\times$ and $2\times$ optical objectives for higher resolution and larger field of view, respectively. The diffracted beam was focused and the image was magnified by an X-ray objective lens (2D CRLs). The objective CRLs provided an image of the diffracting grain onto the far-field detector, with an X-ray magnification of $M_x = 17.9\times$, leading to a spatial resolution of $\approx 125\ \text{nm}$ using the $10\times$ objective. To obtain 3D information, DFXM images were collected in 2D layers, scanning the sample in the vertical direction, z , to resolve the variation along the height of the crystal with $1\ \mu\text{m}/\text{step}$ for scans using the $10\times$ objective, and $3\ \mu\text{m}/\text{step}$ for scans using the $2\times$ objective, respectively. The orientation and strain maps were collected as 2D meshes of the sample tilts and the 2θ around the 111 scattering vector (Figure 2(a)). The DFXM data were analyzed using the *darfix* and in-house built MATLAB scripts [24]. The matching of the GOI for EBSD and DFXM measurements was enabled by a DCT scan on the sample (see the Supp. Mat. for details).

A typical DFXM mosaicity map (a mesh of two sample tilts, ω , and χ) is shown in Figure 2(b) from an interior slice ($30\ \mu\text{m}$ below the surface) of the GOI. The overall shape of the grain is elongated, which correlates with the EBSD observations. At the same time, the DFXM results display unique features in the LAM microstructure when compared to the EBSD measurements. Within the mapped layers, elongated band-like structures with similar local orientations are observed to align parallel to each other. Those structures most likely to follow the laser traverse/heat transfer direction of the manufacturing process. The overall angular spread of the GOI is less than 1.2° .

The band-like structures aligned across the length of the grain show $\approx 0.3\text{-}0.5^\circ$ misorientation from one another, while in the interior they consist of cells with diameters $< 5\text{ }\mu\text{m}$. Fig. 2 (c) shows the map of the misorientation; defined by $\Delta\gamma = \sqrt{(\Delta\omega)^2 + (\Delta\chi)^2}$ [25, 26]. Here, $\Delta\omega$ and $\Delta\chi$ are the differences between the local sample tilt center-of-mass and their grain averages [24]. Figure 2(c) and (d) show $\approx 5\text{ }\mu\text{m}$ -sized subgrains having boundaries with high dislocation densities at a layer $3\text{ }\mu\text{m}$ deep below the surface of the grain. The calculated dislocation densities using DFXM are found to be on the same order of magnitude as the EBSD measurements shown in Figure 2(e).

Probing deeper into the bulk, Figure 3 shows a higher resolution DFXM orientation maps of a layer embedded $30\text{ }\mu\text{m}$ below the surface of the sample, collected using the $10\times$ objective. In Figure 3(a), the χ center-of-mass map shows distinct subgrains separated with low-angle grain boundaries. The overall angular spread in this map reaches up to 1° . Looking at the misorientation map (Figure 3(b)), boundaries along the length of the grain (the band-like structure) with $\approx 0.15^\circ$ misorientation are observed. The magnified image in Figure 3(c) shows two of these structures (denoted by dashed lines) around $5\text{ }\mu\text{m}$ apart (one cell is marked with the dashed shape). For comparison, the Kernel Average Misorientation (KAM) from the EBSD dataset had a mean and standard deviation of 0.045° and 0.028° , respectively (see Figure 1(d)).

It is suspected that these intragranular structures may be a result of a combination of the stresses that build up due to the high cooling rates and the chemical segregation (solutes and carbides) during the fabrication [27]. In an earlier study on the same alloy (ABD-900AM), it was shown that Ti atoms segregate to local cell boundaries at a smaller scale ($\approx 750\text{ nm}$ -sized cells) in the as-fabricated state [28]. When looking closely at our DFXM results, similar boundaries can be seen as lines of 0.1° misorientation $\sim 400\text{-}800\text{ nm}$ range between (see yellow arrows in Figure 3(c)).

Going beyond the complex microstructures in a given 2D layer within the volume, we now turn to the 3D structure of the GOI in Figure 4. The 3D structure of the grain displays significant heterogeneity in the local orientation. We observe orientation bands extending from the surface towards the interior of the grain, spanning more than $50\text{ }\mu\text{m}$. All three of the 2D slices, (xy , yz , and xz , Figure 4(c)), from the 3D volume, show rather sharp orientation changes, compared to smooth and gradual changes observed in highly-deformed metals [25]. This may be due to the pinning effect of the chemical segregation on the dislocations, making them less mobile during the cooling thus creating well-separated boundaries with measurable orientation differences less than 0.5° . Recently, using DFXM we found that even low concentrations (below 0.1%) of solute elements can have a significant dragging effect on the mobility of dislocations, especially for loops, even at high-temperature annealing[29]. For superalloys such segrega-

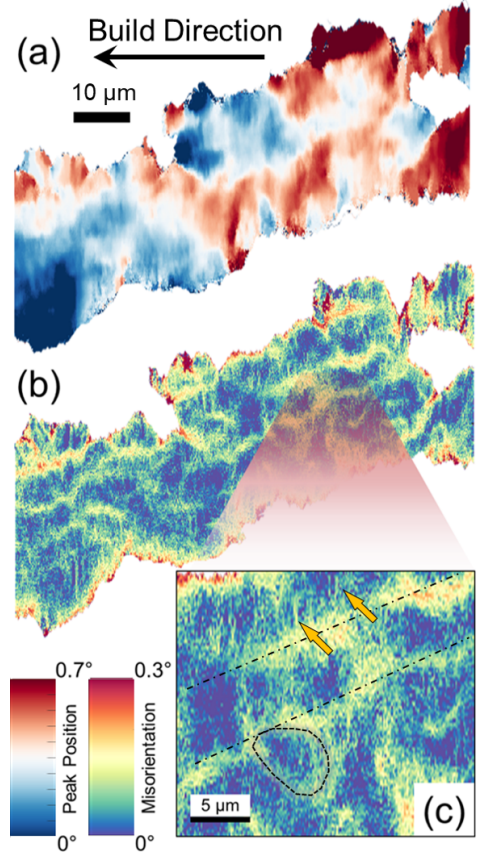


Figure 3: (a) DFXM sample orientation χ peak position center of the mass map of a given layer. The color scale range is chosen such that the contrast is maximized. (b) Calculated high resolution (using the $10\times$ objective) misorientation map of the same layer. (c) Magnified region of the misorientation map emphasizing the cell boundaries.

tion has been associated, for example, with pipe diffusion during creep [30]. Note that all the slices shown in Figure 4(c)) have different morphologies. This indicates the cooling gradients during the fabrication are anisotropic, causing a heterogenous 3D orientation distribution and thus resulting in anisotropic mechanical properties [31, 28].

Similar to the single-slice observation in Figure 2(b), distinct band-like cell structures with similar orientations exist in all slices in Figure 4(d). Inside the bands, an orientation distribution is also observed in the shape of cell structures. These structures are visible thanks to the high angular resolution of the DFXM, which can reveal subtle orientation variations that are otherwise impossible to observe with EBSD [32]. These variations near the subgrain boundaries are likely due to the presence of a higher dislocation density than the surrounding matrix, specifically geometrically necessary dislocations (GNDs) caused by lattice distortions. Note that DFXM measures only certain lattice curvature components (i.e. only one Bragg peak is measured, $\text{GND}_{[111]}$), thus the magnitude of the GNDs is underestimated. The local orientation distributions over the measured volume are far from homogeneous (see Supplementary Figure S3.) This is attributed to the complex cooling gradients during manufacturing.

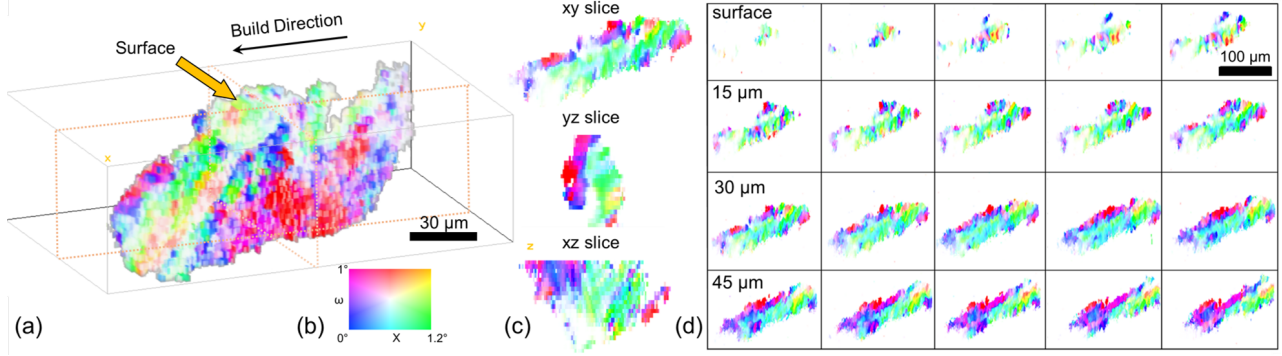


Figure 4: 3D DFXM mosaicity maps of the LAM GOI. (a) 3D reconstruction of 2D layers showing the morphology of the grain. (b) Orientation colour key around a local 111 pole figure for the mosaicity maps. (c) different cut slices from the 3D structure at the mid-layer shown with dashed lines in the 3D reconstruction. (d) (a) 2D DFXM mosaicity maps show the structural heterogeneity across the depth of the grain from surface to interior. Each slice is 3 μm deeper than the previous slice.

The observed lattice distortions should also be considered in connection with the residual stresses. The spread of the relative elastic strain of a given layer is shown in Figure 5(a), demonstrating zones that have highly-accumulated residual strain. The measured strain component is perpendicular to the [111] direction with $\approx 10.15^\circ$ offset. At first glance, the strain distribution is fairly distinctive around the cell structure and the sub-grains, which matches the observation from the mosaicity and misorientation distribution. The misorientation maps suggest that a significantly high dislocation content creates the cell structures, with distinct orientation and strain states. A closer look at the DFXM strain map in Figure 5(a) reveals zones with alternating compressive and tensile strain. These $\approx 5 \mu\text{m}$ -sized zones correspond well to the cell structures with distinct local orientations, indicating a coupling of the lattice distortion and the d-spacing change in the interior of the grain. However, the finer structures which may be linked to the solute segregation (i.e. Ti [28] in Figure 3(c)) are not visible in the strain map. Instead, a rather homogeneous strain distribution is observed within these cells that are aligned along the length of the grain with alternating strain states. Moreover, high strains (>0.003) are observed around the grain boundaries (marked with yellow arrows). This is attributed to the constraining effect of the neighboring grains during the solidification, creating stress concentration zones around the grain boundaries. Using the $\{111\}$ diffraction elastic constant of a similar alloy[33], it is found that these zones may have stresses extending to 850 MPa; on the order of the yield stress of the alloy[18](See the Supplementary Figure S4). In addition, the strain fields of these highly-stressed zones propagate toward the interior of the grain, increasing the overall residual stress level (marked by the red arrow and the ellipse). The stored energy created by the high residual stresses and the high dislocation density can trigger static recrystallization and should be considered for subsequent anisotropy-removing recrystallization and γ' transformation heat treatments.

Figure 5(b) shows the residual elastic strain obtained

from the EBSD measurements, rotated from the sample reference frame into the [111] direction (method in [34]), for direct comparison to the DFXM dataset. The map shows significant deformation patterning within the GOI, forming cell-type structures of compressive or tensile strain. This cell size approximately matches those observed in the DFXM strain map in Figure 5(a), indicating these features can be resolved by both techniques. Although the measured strain magnitudes are similar between the two techniques, EBSD maps do not reveal the clear alternating tension and compression patterning. This may be due to the strain relaxation at the surface. A feature which is, however, common to both is a band of tensile strain that runs parallel to the length of the grain, as indicated by the green arrows. Figure 5(c) shows a heterogeneous distribution of the lattice strain within the measured volume. Although the magnitude of the strain decreases at the surface where relaxation is expected, the strain spread shown in Figure 5(d) shows an increase closer to the surface (region marked by the red color). This deviation from the surface to the interior ranging over some tens of micrometers is likely to be due to the polishing effects on the surface when the sample was prepared for the EBSD measurements prior to the DFXM experiment.

A clear picture now emerges of how the observed complex intragranular microstructures are formed via DED-LAM technique in the ABD-900AM alloy. During solidification, large volume changes that occur due to the phase transformation give rise to the generation of many dislocations in order to accommodate the volume differences [35]. These dislocations are predominantly GNDs, creating intragranular cells with low-angle grain boundaries, manifesting themselves as measurable misorientation in the mosaicity scans. Due to the limited time spent at high temperatures during LAM, small cells with various sizes below $5 \mu\text{m}$ are formed, unlike their cast counterparts[36]. The cell sizes remain small because of the low mobility of the dislocations caused by the combined effect of the rapid cooling and the chemical segregation of the solute atoms and carbides[28]. The DFXM strain scans show that the

effective d-spacing changes during solidification, resulting in prominent stresses around the grain boundaries as a result of the contact with neighboring grains during the fabrication process. Some of these stresses extend tens of micrometers toward the interior of the grain. As the strain distribution within the intragranular cells is homogeneous with clear alternation of tension and compression zones from cell to cell, we argue that the strain distribution within the cells is dominated by the thermal effects rather than the chemical effect.

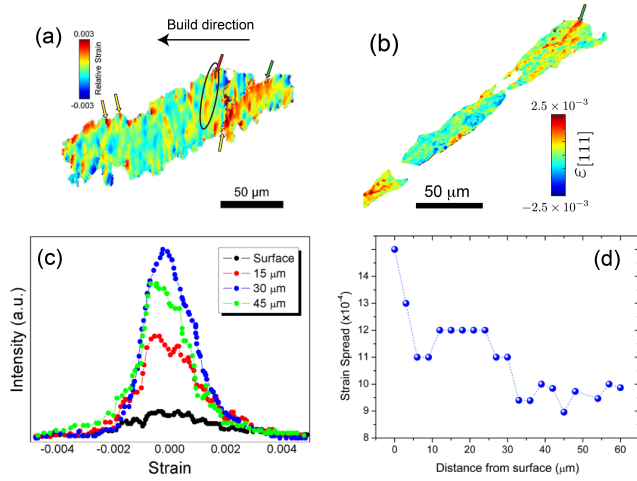


Figure 5: DFXM relative strain maps of a LAM grain. (a) DFXM relative axial strain map of a slice 30 μm below the surface of the grain. (b) Calculated residual elastic strain, resolved into the $[111]$ direction, obtained from the EBSD measurements. (c) DFXM-measured strain distribution at different depths of the grain. (d) Total DFXM-measured strain spread as a function of distance from the surface of the grain. Note that the term strain spread indicates the width of the strain distribution around the local d_0 value of the grain for each layer.

The present study demonstrated subsurface variations of the local strain and orientation of a surface-breaking grain in an additively-manufactured sample using DFXM. The DFXM method successfully resolves complex 3D networks of a highly-strained grain in the as fabricated state, non-destructively revealing the deformation substructure patterning that cannot be resolved by other techniques in bulk. We compare the DFXM results to the EBSD measurements of the same grain. Our results show that band-like structures aligned along the length of the grain and $\approx 5 \mu\text{m}$ -sized cell structures within these bands are formed due to the extreme thermal gradients during LAM, and that they are aligned towards the build direction along the length of the grain. At a finer length scale, misorientation lines of 400-800 nm connecting larger cell structures are observed. These lines were attributed to the chemical segregation, based on a recent study on the same alloy[28]. 3D DFXM strain and orientation maps show that distortion patterning and magnitudes within an individual grain vary significantly (on the order of several micrometers). This demonstrates that DFXM provides representative bulk information of complex subsurface microplasticity for mate-

rials fabricated via LAM. Our DFXM results provide unprecedented 3D intragranular information on the lattice strain and distortion, opening up new avenues not only for potential improvements in the design of heat treatment routes and future experiments for *in-situ* manufacturing, but also for new input parameters for modeling such as geometrical boundary conditions, misorientation angles, and strain fields.

Acknowledgements

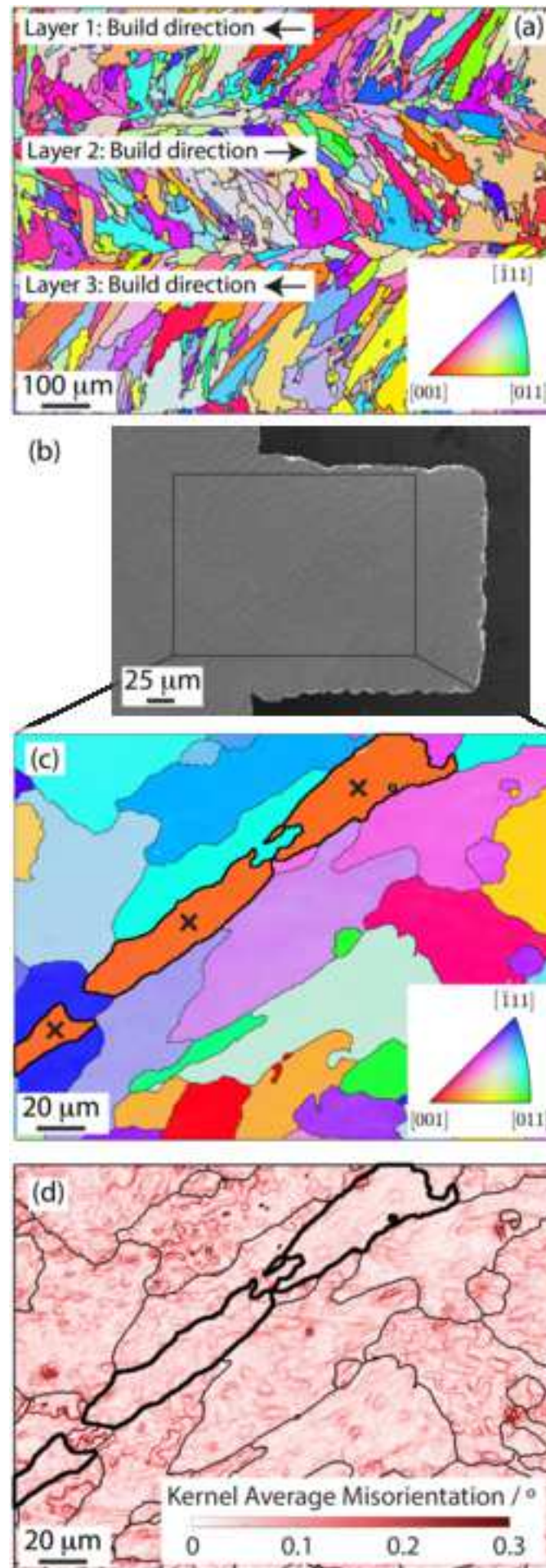
We thank the ESRF for the provision of beamtime at ID06-HXM and ID11. YC acknowledges the support from the RMIT Vice Chancellor's Senior Research Fellowship. PJW and YT acknowledge support from the European Research Council Grant No 695638. The authors are grateful to Alloyed Ltd for the provision of material. This research used resources of the Advanced Photon Source, a U.S. Department of Energy (DOE) Office of Science user facility at Argonne National Laboratory, and is based on research supported by the U.S. DOE Office of Science-Basic Energy Sciences, under Contract No. DE-AC02-06CH11357.

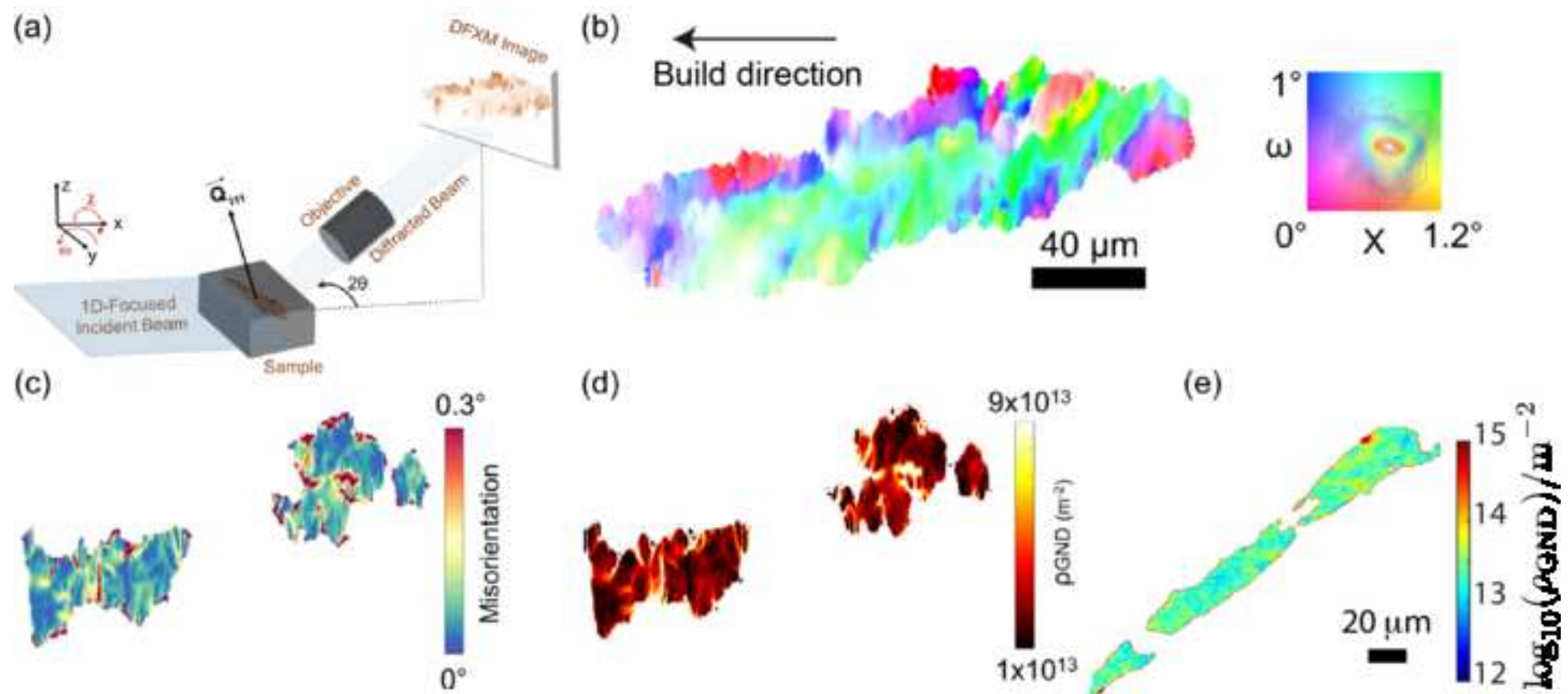
References

- [1] D. D. Gu, W. Meiners, K. Wissenbach, R. Poprawe, Laser additive manufacturing of metallic components: materials, processes and mechanisms, International materials reviews 57 (3) (2012) 133–164.
- [2] P. A. Hooper, Melt pool temperature and cooling rates in laser powder bed fusion, Additive Manufacturing 22 (2018) 548–559.
- [3] O. Fergani, F. Berto, T. Welo, S. Liang, Analytical modelling of residual stress in additive manufacturing, Fatigue & Fracture of Engineering Materials & Structures 40 (6) (2017) 971–978.
- [4] C. Li, Z. Liu, X. Fang, Y. Guo, Residual stress in metal additive manufacturing, Procedia Cirp 71 (2018) 348–353.
- [5] Q. Wang, S. Zhang, C. Zhang, C. Wu, J. Wang, J. Chen, Z. Sun, Microstructure evolution and ebsd analysis of a graded steel fabricated by laser additive manufacturing, Vacuum 141 (2017) 68–81.
- [6] O. Gokcekaya, N. Hayashi, T. Ishimoto, K. Ueda, T. Narushima, T. Nakano, Crystallographic orientation control of pure chromium via laser powder bed fusion and improved high temperature oxidation resistance, Additive Manufacturing 36 (2020) 101624.
- [7] M. K. Alam, M. Mehdi, R. J. Urbanic, A. Edrissy, Electron backscatter diffraction (ebstd) analysis of laser-cladded aisi 420 martensitic stainless steel, Materials Characterization 161 (2020) 110138.
- [8] J. R. Hönnige, P. Colegrove, S. Williams, Improvement of microstructure and mechanical properties in wire+ arc additively manufactured ti-6al-4v with machine hammer peening, Procedia engineering 216 (2017) 8–17.
- [9] C. Zhao, K. Fezzaa, R. W. Cunningham, H. Wen, F. De Carlo, L. Chen, A. D. Rollett, T. Sun, Real-time monitoring of laser powder bed fusion process using high-speed x-ray imaging and diffraction, Scientific reports 7 (1) (2017) 1–11.
- [10] C. L. A. Leung, S. Marussi, R. C. Atwood, M. Towrie, P. J. Withers, P. D. Lee, In situ x-ray imaging of defect and molten pool dynamics in laser additive manufacturing, Nature communications 9 (1) (2018) 1–9.
- [11] Y. Chen, S. J. Clark, L. Sinclair, C. L. A. Leung, S. Marussi, T. Connolly, R. C. Atwood, G. J. Baxter, M. A. Jones, I. Todd, et al., Synchrotron x-ray imaging of directed energy deposition

- additive manufacturing of titanium alloy ti-6242, *Additive Manufacturing* 41 (2021) 101969.
- [12] A. Thompson, I. Maskery, R. K. Leach, X-ray computed tomography for additive manufacturing: a review, *Measurement Science and Technology* 27 (7) (2016) 072001.
- [13] S. J. Wolff, H. Wang, B. Gould, N. Parab, Z. Wu, C. Zhao, A. Greco, T. Sun, In situ x-ray imaging of pore formation mechanisms and dynamics in laser powder-blown directed energy deposition additive manufacturing, *International Journal of Machine Tools and Manufacture* 166 (2021) 103743.
- [14] V. Prithivirajan, P. Ravi, D. Naragani, M. D. Sangid, Direct comparison of microstructure-sensitive fatigue crack initiation via crystal plasticity simulations and in situ high-energy x-ray experiments, *Materials & Design* 197 (2021) 109216.
- [15] W. Ludwig, S. Schmidt, E. M. Lauridsen, H. F. Poulsen, X-ray diffraction contrast tomography: a novel technique for three-dimensional grain mapping of polycrystals. i. direct beam case, *Journal of Applied Crystallography* 41 (2) (2008) 302–309.
- [16] H. Simons, A. King, W. Ludwig, C. Detlefs, W. Pantleon, S. Schmidt, F. Stöhr, I. Snigireva, A. Snigirev, H. F. Poulsen, Dark-field x-ray microscopy for multiscale structural characterization, *Nature Communications* 6 (1) (2015) 6098. doi:10.1038/ncomms7098.
- [17] C. Yildirim, P. Cook, C. Detlefs, H. Simons, H. F. Poulsen, Probing nanoscale structure and strain by dark-field x-ray microscopy, *MRS Bulletin* 45 (4) (2020) 277–282.
- [18] Y. T. Tang, J. N. Ghoussoub, C. Panwisawas, D. M. Collins, S. Amirkhanlou, J. W. Clark, A. A. Németh, D. Graham McCartney, R. C. Reed, The effect of heat treatment on tensile yielding response of the new superalloy abd-900am for additive manufacturing, in: *Superalloys 2020*, Springer, 2020, pp. 1055–1065.
- [19] A. J. Wilkinson, T. B. Britton, Strains, planes, and ebsd in materials science, *Materials today* 15 (9) (2012) 366–376.
- [20] B. Britton, I. Holton, G. Meaden, D. Dingley, High angular resolution electron backscatter diffraction: measurement of strain in functional and structural materials, *Microscopy and Analysis* 27 (4) (2013) 8.
- [21] A. Wilkinson, G. Meaden, D. Dingley, High resolution mapping of strains and rotations using electron backscatter diffraction, *Mater. Sci Tech.* 22 (2006) 1271–1278.
- [22] A. J. Wilkinson, G. Meaden, D. J. Dingley, High-resolution elastic strain measurement from electron backscatter diffraction patterns: New levels of sensitivity, *Ultramicroscopy* 106 (4-5) (2006) 307–313.
- [23] M. Kutsal, P. Bernard, G. Berruyer, P. K. Cook, R. Hino, A. C. Jakobsen, W. Ludwig, J. Ormstrup, T. Roth, H. Simons, K. Smets, J. X. Sierra, J. Wade, P. Wattecamps, C. Yildirim, H. F. Poulsen, C. Detlefs, The esrf dark-field x-ray microscope at id06, *IOP Conference Series: Materials Science and Engineering* 580 (2019) 012007.
- [24] J. Garriga Ferrer, et al., darfix: Data analysis for dark-field x-ray microscopy, *Journal of Synchrotron Radiation* 30 (2023).
- [25] C. Yildirim, N. Mavrikakis, P. Cook, R. Rodriguez-Lamas, M. Kutsal, H. Poulsen, C. Detlefs, 4d microstructural evolution in a heavily deformed ferritic alloy: A new perspective in recrystallisation studies, *Scripta Materialia* 214 (2022) 114689.
- [26] C. Yildirim, N. Mavrikakis, P. Cook, R. R. Lamas, H. Poulsen, C. Detlefs, M. Kutsal, Multiscale exploration of texture and microstructure development in recrystallization annealing of heavily deformed ferritic alloys, in: *IOP Conference Series: Materials Science and Engineering*, Vol. 1249, IOP Publishing, 2022, p. 012044.
- [27] A. Hariharan, L. Lu, J. Risse, A. Kostka, B. Gault, E. A. Jägle, D. Raabe, Misorientation-dependent solute enrichment at interfaces and its contribution to defect formation mechanisms during laser additive manufacturing of superalloys, *Phys. Rev. Materials* 3 (2019) 123602. doi:10.1103/PhysRevMaterials.3.123602.
- [28] Y. T. Tang, C. Panwisawas, B. M. Jenkins, J. Liu, Z. Shen, E. Salvati, Y. Gong, J. N. Ghoussoub, S. Michalik, B. Roebuck, et al., Multi-length-scale study on the heat treatment response to supersaturated nickel-based superalloys: Precipitation reactions and incipient recrystallisation, *Additive Manufacturing* (2023) 103389.
- [29] N. Mavrikakis, C. Detlefs, P. Cook, M. Kutsal, A. Campos, M. Gauvin, P. Calvillo, W. Saikaly, R. Hubert, H. F. Poulsen, et al., A multi-scale study of the interaction of sn solutes with dislocations during static recovery in α -fe, *Acta Materialia* 174 (2019) 92–104.
- [30] P. Kontis, Z. Li, D. M. Collins, J. Cormier, D. Raabe, B. Gault, The effect of chromium and cobalt segregation at dislocations on nickel-based superalloys, *Scripta Materialia* 145 (2018) 76–80.
- [31] R. Muñoz-Moreno, V. Divya, S. Driver, O. Messé, T. Illston, S. Baker, M. Carpenter, H. Stone, Effect of heat treatment on the microstructure, texture and elastic anisotropy of the nickel-based superalloy cm247lc processed by selective laser melting, *Materials Science and Engineering: A* 674 (2016) 529–539.
- [32] K. Hlushko, J. Keckes, G. Ressel, J. Pörnbacher, W. Ecker, M. Kutsal, P. Cook, C. Detlefs, C. Yildirim, Dark-field x-ray microscopy reveals mosaicity and strain gradients across sub-surface tic and tin particles in steel matrix composites, *Scripta Materialia* 187 (2020) 402–406.
- [33] P. Aba-Perea, T. Pirling, P. Withers, J. Kelleher, S. Kabra, M. Preuss, Determination of the high temperature elastic properties and diffraction elastic constants of ni-base superalloys, *Materials & Design* 89 (2016) 856–863.
- [34] Y. T. Tang, N. D’Souza, B. Roebuck, P. Karamched, C. Panwisawas, D. M. Collins, Ultra-high temperature deformation in a single crystal superalloy: Mesoscale process simulation and micromechanisms, *Acta Materialia* 203 (2021) 116468.
- [35] T. DeRoy, H. Wei, J. Zuback, T. Mukherjee, J. Elmer, J. Milewski, A. M. Beese, A. d. Wilson-Heid, A. De, W. Zhang, Additive manufacturing of metallic components—process, structure and properties, *Progress in Materials Science* 92 (2018) 112–224.
- [36] M. Jahangiri, S. Boutorabi, H. Arabi, Study on incipient melting in cast ni base in939 superalloy during solution annealing and its effect on hot workability, *Materials Science and Technology* 28 (12) (2012) 1402–1413.







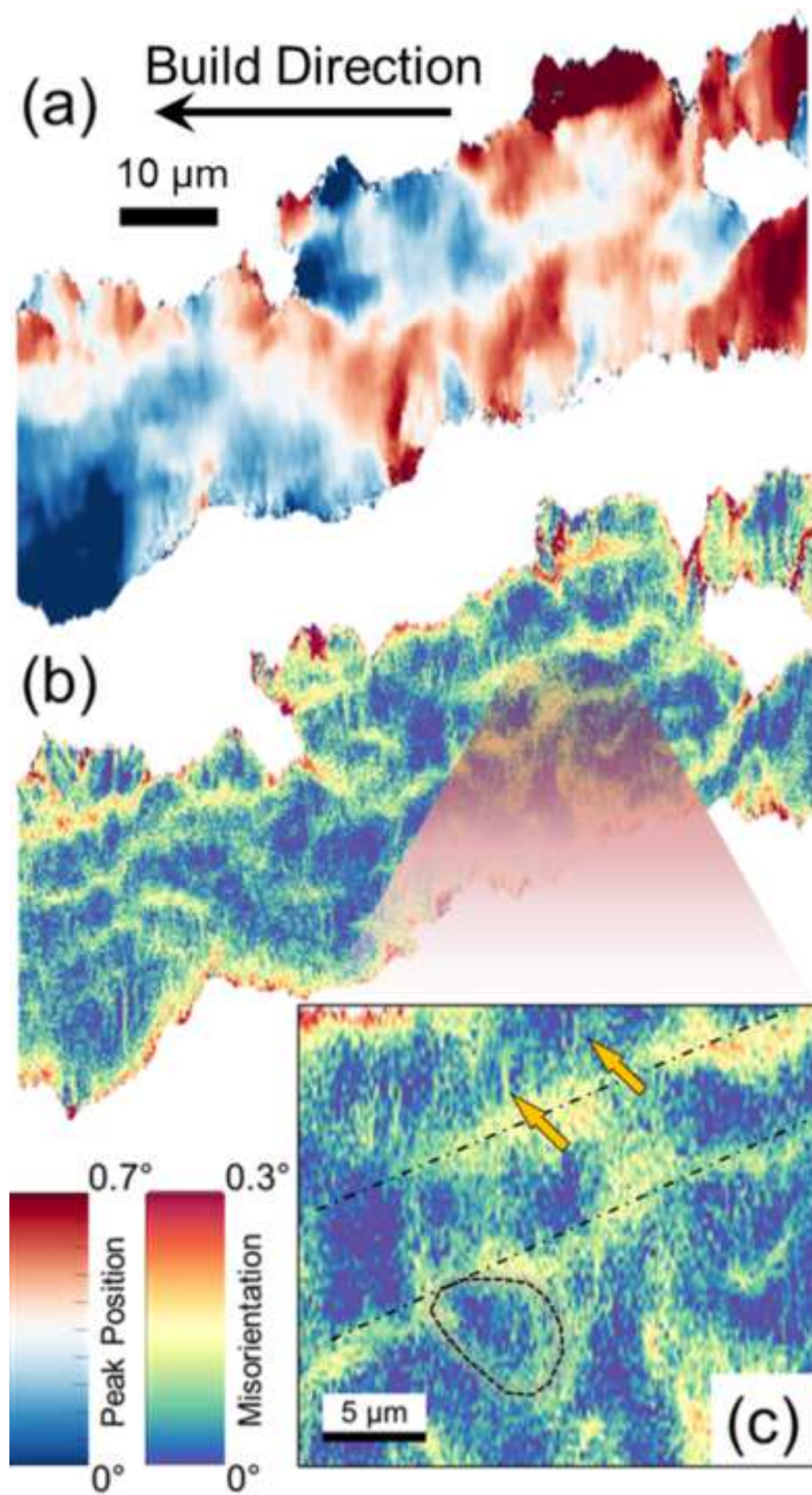
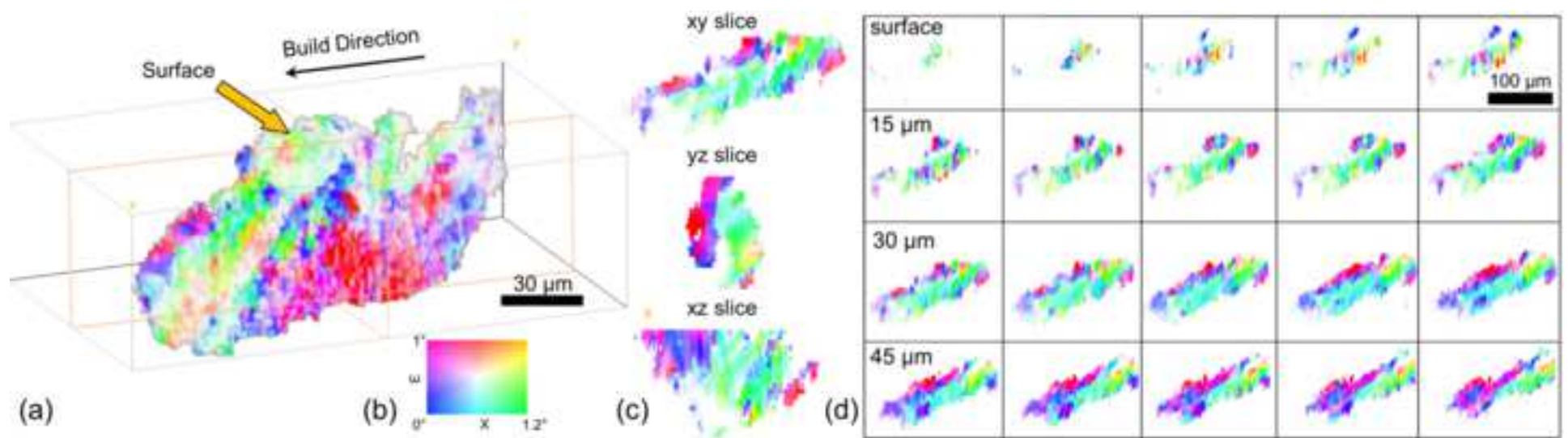
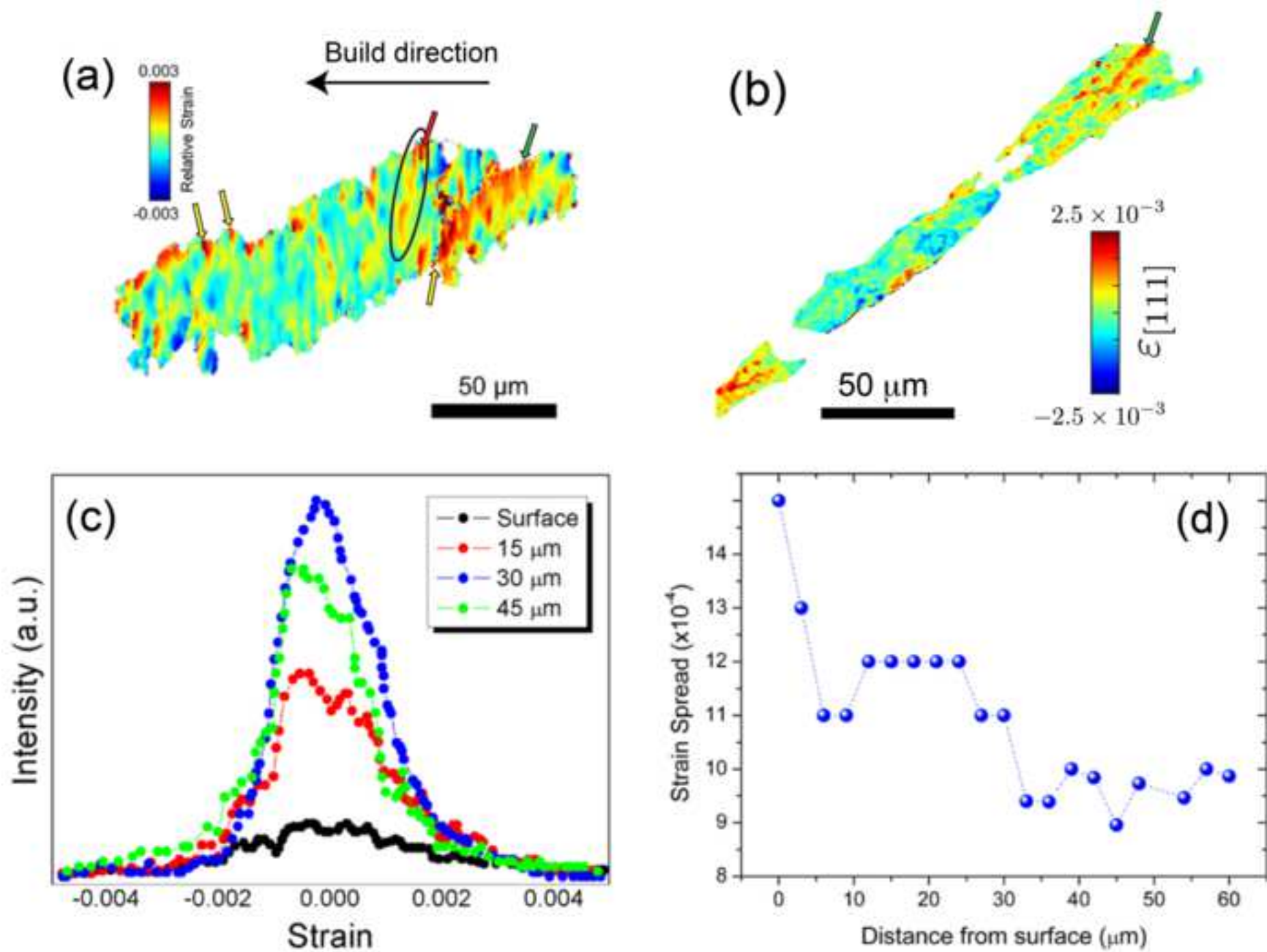


Figure4





Declaration of interests

☒ The authors declare that they have no known competing financial interests or personal relationships that could have appeared to influence the work reported in this paper.

☐The authors declare the following financial interests/personal relationships which may be considered as potential competing interests:


```
1
2
3
4 This is pdfTeX, Version 3.141592653-2.6-1.40.24 (TeX Live 2022)
5 (preloaded format=pdflatex 2023.3.8) 17 MAY 2023 23:59
6 entering extended mode
7 restricted \writel8 enabled.
8 %&-line parsing enabled.
9 **main_scripta_rev.tex
10 (./main_scripta_rev.tex
11 LaTeX2e <2022-11-01> patch level 1
12 L3 programming layer <2023-02-22> (c:/TeXLive/2022/texmf-
13 dist/tex/latex/elsarti
14 cle/elsarticle.cls
15 Document Class: elsarticle 2020/11/20, 3.3: Elsevier Ltd
16 (c:/TeXLive/2022/texmf-dist/tex/latex/l3kernel/expl3.sty
17 Package: expl3 2023-02-22 L3 programming layer (loader)
18 (c:/TeXLive/2022/texmf-dist/tex/latex/l3backend/l3backend-pdftex.def
19 File: l3backend-pdftex.def 2023-01-16 L3 backend support: PDF output
20 (pdfTeX)
21 \l__color_backend_stack_int=\count185
22 \l__pdf_internal_box=\box51
23 )) (c:/TeXLive/2022/texmf-dist/tex/latex/l3packages/xparse/xparse.sty
24 Package: xparse 2023-02-02 L3 Experimental document command parser
25 ) (c:/TeXLive/2022/texmf-dist/tex/latex/etoolbox/etoolbox.sty
26 Package: etoolbox 2020/10/05 v2.5k e-TeX tools for LaTeX (JAW)
27 \etb@tempcnta=\count186
28 )
29 \@bls=\dimen140
30 (c:/TeXLive/2022/texmf-dist/tex/latex/base/article.cls
31 Document Class: article 2022/07/02 v1.4n Standard LaTeX document class
32 (c:/TeXLive/2022/texmf-dist/tex/latex/base/size10.clo
33 File: size10.clo 2022/07/02 v1.4n Standard LaTeX file (size option)
34 )
35 \c@part=\count187
36 \c@section=\count188
37 \c@subsection=\count189
38 \c@subsubsection=\count190
39 \c@paragraph=\count191
40 \c@subparagraph=\count192
41 \c@figure=\count193
42 \c@table=\count194
43 \abovecaptionskip=\skip48
44 \belowcaptionskip=\skip49
45 \bibindent=\dimen141
46 ) (c:/TeXLive/2022/texmf-dist/tex/latex/graphics/graphicx.sty
47 Package: graphicx 2021/09/16 v1.2d Enhanced LaTeX Graphics (DPC,SPQR)
48 (c:/TeXLive/2022/texmf-dist/tex/latex/graphics/keyval.sty
49 Package: keyval 2022/05/29 v1.15 key=value parser (DPC)
50 \KV@toks@=\toks16
51 ) (c:/TeXLive/2022/texmf-dist/tex/latex/graphics/graphics.sty
52 Package: graphics 2022/03/10 v1.4e Standard LaTeX Graphics (DPC,SPQR)
53 (c:/TeXLive/2022/texmf-dist/tex/latex/graphics/trig.sty
54 Package: trig 2021/08/11 v1.11 sin cos tan (DPC)
55 ) (c:/TeXLive/2022/texmf-dist/tex/latex/graphics-cfg/graphics.cfg
56 File: graphics.cfg 2016/06/04 v1.11 sample graphics configuration
57 )
58
59
60
61
62
63
64
65
```

```

1
2
3
4 Package graphics Info: Driver file: pdftex.def on input line 107.
5 (c:/TeXLive/2022/texmf-dist/tex/latex/graphics-def/pdftex.def
6 File: pdftex.def 2022/09/22 v1.2b Graphics/color driver for pdftex
7 ))
8 \Gin@req@height=\dimen142
9 \Gin@req@width=\dimen143
10 )
11 \c@tnote=\count195
12 \c@fnote=\count196
13 \c@cnote=\count197
14 \c@ead=\count198
15 \c@author=\count199
16 \@eadauthor=\toks17
17 \c@affn=\count266
18 \absbox=\box52
19 \elsarticlehighlightsbox=\box53
20 \elsarticlegrabsbox=\box54
21 \keybox=\box55
22 \Columnwidth=\dimen144
23 \space@left=\dimen145
24 \els@boxa=\box56
25 \els@boxb=\box57
26 \leftMargin=\dimen146
27 \@enLab=\toks18
28 \@sep=\skip50
29 @@sep=\skip51
30 (./main_scripta_rev.spl) (c:/TeXLive/2022/texmf-
31 dist/tex/latex/natbib/natbib.st
32 Y
33 Package: natbib 2010/09/13 8.31b (PWD, AO)
34 \bibhang=\skip52
35 \bibsep=\skip53
36 LaTeX Info: Redefining \cite on input line 694.
37 \c@NAT@ctr=\count267
38 )
39 \splwrite=\write3
40 \openout3 = `main_scripta_rev.spl'.
41
42 (c:/TeXLive/2022/texmf-dist/tex/latex/geometry/geometry.sty
43 Package: geometry 2020/01/02 v5.9 Page Geometry
44 (c:/TeXLive/2022/texmf-dist/tex/generic/iftex/ifvtex.sty
45 Package: ifvtex 2019/10/25 v1.7 ifvtex legacy package. Use iftex instead.
46 (c:/TeXLive/2022/texmf-dist/tex/generic/iftex/iftex.sty
47 Package: iftex 2022/02/03 v1.0f TeX engine tests
48 ))
49 \Gm@cnth=\count268
50 \Gm@cntv=\count269
51 \c@Gm@tempcnt=\count270
52 \Gm@bindingoffset=\dimen147
53 \Gm@wd@mp=\dimen148
54 \Gm@odd@mp=\dimen149
55 \Gm@even@mp=\dimen150
56 \Gm@layoutwidth=\dimen151
57 \Gm@layoutheight=\dimen152
58
59
60
61
62
63
64
65

```



```

\Gm@layouthoffset=\dimen153
\Gm@layoutvoffset=\dimen154
\Gm@dimlist=\toks19
) (c:/TeXLive/2022/texmf-dist/tex/latex/base/flegn.clo
File: flegn.clo 2016/12/29 v1.2b Standard LaTeX option (flush left
equations)
\mathindent=\skip54
Applying: [2015/01/01] Make \[ robust on input line 50.
LaTeX Info: Redefining \[ on input line 51.
Already applied: [0000/00/00] Make \[ robust on input line 62.
Applying: [2015/01/01] Make \] robust on input line 74.
LaTeX Info: Redefining \] on input line 75.
Already applied: [0000/00/00] Make \] robust on input line 83.
)
\appnamewidth=\dimen155
) (c:/TeXLive/2022/texmf-dist/tex/latex/txfonts/txfonts.sty
Package: txfonts 2008/01/22 v3.2.1
LaTeX Font Info: Redefining symbol font `operators' on input line 21.
LaTeX Font Info: Overwriting symbol font `operators' in version
`normal'
(Font) OT1/cmr/m/n --> OT1/txr/m/n on input line 21.
LaTeX Font Info: Overwriting symbol font `operators' in version `bold'
(Font) OT1/cmr/bx/n --> OT1/txr/m/n on input line 21.
LaTeX Font Info: Overwriting symbol font `operators' in version `bold'
(Font) OT1/txr/m/n --> OT1/txr/bx/n on input line 22.
\symitalic=\mathgroup4
LaTeX Font Info: Overwriting symbol font `italic' in version `bold'
(Font) OT1/txr/m/it --> OT1/txr/bx/it on input line 26.
LaTeX Font Info: Redefining math alphabet \mathbf on input line 29.
LaTeX Font Info: Overwriting math alphabet ``\mathbf' in version
`normal'
(Font) OT1/cmr/bx/n --> OT1/txr/bx/n on input line 29.
LaTeX Font Info: Overwriting math alphabet ``\mathbf' in version `bold'
(Font) OT1/cmr/bx/n --> OT1/txr/bx/n on input line 29.
LaTeX Font Info: Redefining math alphabet \mathit on input line 30.
LaTeX Font Info: Overwriting math alphabet ``\mathit' in version
`normal'
(Font) OT1/cmr/m/it --> OT1/txr/m/it on input line 30.
LaTeX Font Info: Overwriting math alphabet ``\mathit' in version `bold'
(Font) OT1/cmr/bx/it --> OT1/txr/m/it on input line 30.
LaTeX Font Info: Overwriting math alphabet ``\mathit' in version `bold'
(Font) OT1/txr/m/it --> OT1/txr/bx/it on input line 31.
LaTeX Font Info: Redefining math alphabet \mathsf on input line 40.
LaTeX Font Info: Overwriting math alphabet ``\mathsf' in version
`normal'
(Font) OT1/cmss/m/n --> OT1/txss/m/n on input line 40.
LaTeX Font Info: Overwriting math alphabet ``\mathsf' in version `bold'
(Font) OT1/cmss/bx/n --> OT1/txss/m/n on input line 40.
LaTeX Font Info: Overwriting math alphabet ``\mathsf' in version `bold'
(Font) OT1/txss/m/n --> OT1/txss/b/n on input line 41.
LaTeX Font Info: Redefining math alphabet \mathtt on input line 50.
LaTeX Font Info: Overwriting math alphabet ``\mathtt' in version
`normal'
(Font) OT1/cmtd/m/n --> OT1/txtd/m/n on input line 50.

```

```

1
2
3
4 LaTeX Font Info: Overwriting math alphabet '\mathtt' in version 'bold'
5 (Font) OT1/cmtt/m/n --> OT1/txtt/m/n on input line 50.
6 LaTeX Font Info: Overwriting math alphabet '\mathtt' in version 'bold'
7 (Font) OT1/txtt/m/n --> OT1/txtt/b/n on input line 51.
8 LaTeX Font Info: Redefining symbol font 'letters' on input line 58.
9 LaTeX Font Info: Overwriting symbol font 'letters' in version 'normal'
10 (Font) OML/cmm/m/it --> OML/txmi/m/it on input line 58.
11 LaTeX Font Info: Overwriting symbol font 'letters' in version 'bold'
12 (Font) OML/cmm/b/it --> OML/txmi/m/it on input line 58.
13 LaTeX Font Info: Overwriting symbol font 'letters' in version 'bold'
14 (Font) OML/txmi/m/it --> OML/txmi/bx/it on input line
15 59.
16 \symlettersA=\mathgroup5
17 LaTeX Font Info: Overwriting symbol font 'lettersA' in version 'bold'
18 (Font) U/txmia/m/it --> U/txmia/bx/it on input line 67.
19 LaTeX Font Info: Redefining symbol font 'symbols' on input line 77.
20 LaTeX Font Info: Overwriting symbol font 'symbols' in version 'normal'
21 (Font) OMS/cmsy/m/n --> OMS/txsy/m/n on input line 77.
22 LaTeX Font Info: Overwriting symbol font 'symbols' in version 'bold'
23 (Font) OMS/cmsy/b/n --> OMS/txsy/m/n on input line 77.
24 LaTeX Font Info: Overwriting symbol font 'symbols' in version 'bold'
25 (Font) OMS/txsy/m/n --> OMS/txsy/bx/n on input line 78.
26 \symAMSA=\mathgroup6
27 LaTeX Font Info: Overwriting symbol font 'AMSA' in version 'bold'
28 (Font) U/txsya/m/n --> U/txsya/bx/n on input line 94.
29 \symAMSb=\mathgroup7
30 LaTeX Font Info: Overwriting symbol font 'AMSb' in version 'bold'
31 (Font) U/txsyb/m/n --> U/txsyb/bx/n on input line 103.
32 \symsymbolsC=\mathgroup8
33 LaTeX Font Info: Overwriting symbol font 'symbolsC' in version 'bold'
34 (Font) U/txsyc/m/n --> U/txsyc/bx/n on input line 113.
35 LaTeX Font Info: Redefining symbol font 'largesymbols' on input line
36 120.
37 LaTeX Font Info: Overwriting symbol font 'largesymbols' in version
38 'normal'
39 (Font) OMX/cmex/m/n --> OMX/txex/m/n on input line 120.
40 LaTeX Font Info: Overwriting symbol font 'largesymbols' in version
41 'bold'
42 (Font) OMX/cmex/m/n --> OMX/txex/m/n on input line 120.
43 LaTeX Font Info: Overwriting symbol font 'largesymbols' in version
44 'bold'
45 (Font) OMX/txex/m/n --> OMX/txex/bx/n on input line 121.
46 \symlargesymbolsA=\mathgroup9
47 LaTeX Font Info: Overwriting symbol font 'largesymbolsA' in version
48 'bold'
49 (Font) U/txexa/m/n --> U/txexa/bx/n on input line 129.
50 LaTeX Font Info: Redefining math symbol \mathsterling on input line
51 164.
52 LaTeX Font Info: Redefining math symbol \hbar on input line 591.
53 LaTeX Info: Redefining \not on input line 1043.
54 ) (c:/TeXLive/2022/texmf-dist/tex/latex/base/textcomp.sty
55 Package: textcomp 2020/02/02 v2.0n Standard LaTeX package
56 ) (c:/TeXLive/2022/texmf-dist/tex/latex/gensymb/gensymb.sty
57 Package: gensymb 2022/10/17 v1.0.2 (KJH)
58
59
60
61
62
63
64
65

```



```

) (c:/TeXLive/2022/texmf-dist/tex/latex/multirow/multirow.sty
Package: multirow 2021/03/15 v2.8 Span multiple rows of a table
\multirow@colwidth=\skip55
\multirow@cntb=\count271
\multirow@dima=\skip56
\bigstrutjot=\dimen156
) (c:/TeXLive/2022/texmf-dist/tex/latex/float/float.sty
Package: float 2001/11/08 v1.3d Float enhancements (AL)
\c@float@type=\count272
\float@exts=\toks20
\float@box=\box58
\@float@everytoks=\toks21
\@floatcapt=\box59
) (c:/TeXLive/2022/texmf-dist/tex/latex/base/inputenc.sty
Package: inputenc 2021/02/14 v1.3d Input encoding file
\inpenc@prehook=\toks22
\inpenc@posthook=\toks23
(c:/TeXLive/2022/texmf-dist/tex/latex/base/latin1.def
File: latin1.def 2021/02/14 v1.3d Input encoding file
)) (c:/TeXLive/2022/texmf-dist/tex/latex/amsmath/amsmath.sty
Package: amsmath 2022/04/08 v2.17n AMS math features
\@mathmargin=\skip57
For additional information on amsmath, use the '?' option.
(c:/TeXLive/2022/texmf-dist/tex/latex/amsmath/amstext.sty
Package: amstext 2021/08/26 v2.01 AMS text
(c:/TeXLive/2022/texmf-dist/tex/latex/amsmath/amsgen.sty
File: amsgen.sty 1999/11/30 v2.0 generic functions
\@emptytoks=\toks24
\ex@=\dimen157
)) (c:/TeXLive/2022/texmf-dist/tex/latex/amsmath/amsbsy.sty
Package: amsbsy 1999/11/29 v1.2d Bold Symbols
\pmbraise@=\dimen158
) (c:/TeXLive/2022/texmf-dist/tex/latex/amsmath/amsopn.sty
Package: amsopn 2022/04/08 v2.04 operator names
)
\inf@bad=\count273
LaTeX Info: Redefining \frac on input line 234.
\uproot@=\count274
\leftroot@=\count275
LaTeX Info: Redefining \overline on input line 399.
LaTeX Info: Redefining \colon on input line 410.
\classnum@=\count276
\DOTSCASE@=\count277
LaTeX Info: Redefining \ldots on input line 496.
LaTeX Info: Redefining \dots on input line 499.
LaTeX Info: Redefining \cdots on input line 620.
\Mathstrutbox@=\box60
\strutbox@=\box61
LaTeX Info: Redefining \big on input line 722.
LaTeX Info: Redefining \Big on input line 723.
LaTeX Info: Redefining \bigg on input line 724.
LaTeX Info: Redefining \Bigg on input line 725.
\big@size=\dimen159
LaTeX Font Info: Redefining font encoding OML on input line 743.

```

```

LaTeX Font Info:   Redeclaring font encoding OMS on input line 744.
\macc@depth=\count278
LaTeX Info: Redefining \bmod on input line 905.
LaTeX Info: Redefining \pmod on input line 910.
LaTeX Info: Redefining \smash on input line 940.
LaTeX Info: Redefining \relbar on input line 970.
LaTeX Info: Redefining \Relbar on input line 971.
\c@MaxMatrixCols=\count279
\dotsspace@=\muskip16
\c@parentequation=\count280
\dspbrk@lvl=\count281
\tag@help=\toks25
\row@=\count282
\column@=\count283
\maxfields@=\count284
\andhelp@=\toks26
\eqnshift@=\dimen160
\alignsep@=\dimen161
\tagshift@=\dimen162
\tagwidth@=\dimen163
\totwidth@=\dimen164
\lineht@=\dimen165
\@envbody=\toks27
\multlinegap=\skip58
\multlinetaggap=\skip59
\mathdisplay@stack=\toks28
LaTeX Info: Redefining \[ on input line 2953.
LaTeX Info: Redefining \] on input line 2954.
) (c:/TeXLive/texmf-local/tex/latex/aries/epstopdf.sty
Package: epstopdf 2001/02/04 v1.1 Conversion with epstopdf on the fly
(HO)
) (c:/TeXLive/2022/texmf-dist/tex/latex/sttools/flushend.sty
Package: flushend 2021/10/04 v4.0 Balancing columns in twocolumn mode
\flushend@@lastskip@a=\skip60
\flushend@@lastskip@b=\skip61
\flushend@@lastnode=\count285
\var@@loop@iter=\count286
\var@@temp@spread=\dimen166
\var@@temp@a=\dimen167
\var@@temp@loop=\dimen168
\flushend@@page@rule=\dimen169
\flushend@@varbox@lastpage=\box62
\flushend@@varbox@a=\box63
\flushend@@varbox@c=\box64
\flushend@@tempbox@a=\box65
\flushend@@tempbox@c=\box66
\flushend@@floatbox=\box67
\@viper=\box68
\hold@viper=\box69
\atColsBreak=\toks29
\atColsEnd=\toks30
\oldbreak@skip=\dimen170
) (c:/TeXLive/2022/texmf-dist/tex/latex/lm/lmodern.sty
Package: lmodern 2015/05/01 v1.6.1 Latin Modern Fonts

```



```

1
2
3
4 LaTeX Font Info: Overwriting symbol font `operators' in version
5 `normal'
6 (Font) OT1/txr/m/n --> OT1/lmr/m/n on input line 22.
7 LaTeX Font Info: Overwriting symbol font `letters' in version `normal'
8 (Font) OML/txmi/m/it --> OML/lmm/m/it on input line 23.
9 LaTeX Font Info: Overwriting symbol font `symbols' in version `normal'
10 (Font) OMS/txsy/m/n --> OMS/lmsy/m/n on input line 24.
11 LaTeX Font Info: Overwriting symbol font `largesymbols' in version
12 `normal'
13 (Font) OMX/txex/m/n --> OMX/lmex/m/n on input line 25.
14 LaTeX Font Info: Overwriting symbol font `operators' in version `bold'
15 (Font) OT1/txr/bx/n --> OT1/lmr/bx/n on input line 26.
16 LaTeX Font Info: Overwriting symbol font `letters' in version `bold'
17 (Font) OML/txmi/bx/it --> OML/lmm/b/it on input line 27.
18 LaTeX Font Info: Overwriting symbol font `symbols' in version `bold'
19 (Font) OMS/txsy/bx/n --> OMS/lmsy/b/n on input line 28.
20 LaTeX Font Info: Overwriting symbol font `largesymbols' in version
21 `bold'
22 (Font) OMX/txex/bx/n --> OMX/lmex/m/n on input line 29.
23 LaTeX Font Info: Overwriting math alphabet ``\mathbf' in version
24 `normal'
25 (Font) OT1/txr/bx/n --> OT1/lmr/bx/n on input line 31.
26 LaTeX Font Info: Overwriting math alphabet ``\mathsf' in version
27 `normal'
28 (Font) OT1/txss/m/n --> OT1/lmss/m/n on input line 32.
29 LaTeX Font Info: Overwriting math alphabet ``\mathit' in version
30 `normal'
31 (Font) OT1/txr/m/it --> OT1/lmr/m/it on input line 33.
32 LaTeX Font Info: Overwriting math alphabet ``\mathtt' in version
33 `normal'
34 (Font) OT1/txtt/m/n --> OT1/lmtt/m/n on input line 34.
35 LaTeX Font Info: Overwriting math alphabet ``\mathbf' in version `bold'
36 (Font) OT1/txr/bx/n --> OT1/lmr/bx/n on input line 35.
37 LaTeX Font Info: Overwriting math alphabet ``\mathsf' in version `bold'
38 (Font) OT1/txss/b/n --> OT1/lmss/bx/n on input line 36.
39 LaTeX Font Info: Overwriting math alphabet ``\mathit' in version `bold'
40 (Font) OT1/txr/bx/it --> OT1/lmr/bx/it on input line 37.
41 LaTeX Font Info: Overwriting math alphabet ``\mathtt' in version `bold'
42 (Font) OT1/txtt/b/n --> OT1/lmtt/m/n on input line 38.
43 ) (c:/TeXLive/2022/texmf-dist/tex/latex/base/fontenc.sty
44 Package: fontenc 2021/04/29 v2.0v Standard LaTeX package
45 LaTeX Font Info: Trying to load font information for T1+lmr on input
46 line 11
47 2.
48 (c:/TeXLive/2022/texmf-dist/tex/latex/lm/t1lmr.fd
49 File: t1lmr.fd 2015/05/01 v1.6.1 Font defs for Latin Modern
50 )) (c:/TeXLive/2022/texmf-dist/tex/latex/xcolor/xcolor.sty
51 Package: xcolor 2022/06/12 v2.14 LaTeX color extensions (UK)
52 (c:/TeXLive/2022/texmf-dist/tex/latex/graphics-cfg/color.cfg
53 File: color.cfg 2016/01/02 v1.6 sample color configuration
54 )
55 Package xcolor Info: Driver file: pdftex.def on input line 227.
56 (c:/TeXLive/2022/texmf-dist/tex/latex/graphics/mathcolor.ltx)
57
58
59
60
61
62
63
64
65

```

Package xcolor Info: Model `cmy' substituted by `cmy0' on input line 1353.
 Package xcolor Info: Model `hsb' substituted by `rgb' on input line 1357.
 Package xcolor Info: Model `RGB' extended on input line 1369.
 Package xcolor Info: Model `HTML' substituted by `rgb' on input line 1371.
 Package xcolor Info: Model `Hsb' substituted by `hsb' on input line 1372.
 Package xcolor Info: Model `tHsb' substituted by `hsb' on input line 1373.
 Package xcolor Info: Model `HSB' substituted by `hsb' on input line 1374.
 Package xcolor Info: Model `Gray' substituted by `gray' on input line 1375.
 Package xcolor Info: Model `wave' substituted by `hsb' on input line 1376.
) (c:/TeXLive/2022/texmf-dist/tex/latex/was/upgreek.sty
 Package: upgreek 2003/02/12 v2.0 (WaS)
 Package upgreek Info: Using Euler Roman for upright Greek on input line 31.
 \symugrf@m=\mathgroup10
 LaTeX Font Info: Overwriting symbol font `ugrf@m' in version `bold' (Font) U/eur/m/n --> U/eur/b/n on input line 38.
) (c:/TeXLive/2022/texmf-dist/tex/latex/amsfonts/amssymb.sty
 Package: amssymb 2013/01/14 v3.01 AMS font symbols
 (c:/TeXLive/2022/texmf-dist/tex/latex/amsfonts/amsfonts.sty
 Package: amsfonts 2013/01/14 v3.01 Basic AMSFonts support
 LaTeX Font Info: Redefining symbol font `AMSA' on input line 59.
 LaTeX Font Info: Overwriting symbol font `AMSA' in version `normal' (Font) U/txsya/m/n --> U/msa/m/n on input line 59.
 LaTeX Font Info: Overwriting symbol font `AMSA' in version `bold' (Font) U/txsya/bx/n --> U/msa/m/n on input line 59.
 LaTeX Font Info: Redefining symbol font `AMSb' on input line 60.
 LaTeX Font Info: Overwriting symbol font `AMSb' in version `normal' (Font) U/txsyb/m/n --> U/msb/m/n on input line 60.
 LaTeX Font Info: Overwriting symbol font `AMSb' in version `bold' (Font) U/txsyb/bx/n --> U/msb/m/n on input line 60.
 LaTeX Font Info: Redefining math delimiter \ulcorner on input line 74.
 LaTeX Font Info: Redefining math delimiter \urcorner on input line 75.
 LaTeX Font Info: Redefining math delimiter \llcorner on input line 76.
 LaTeX Font Info: Redefining math delimiter \lrcorner on input line 77.
 LaTeX Font Info: Redefining math symbol \square on input line 141.
 LaTeX Font Info: Redefining math symbol \lozenge on input line 142.
)
 LaTeX Font Info: Redefining math symbol \boxdot on input line 44.
 LaTeX Font Info: Redefining math symbol \boxplus on input line 45.
 LaTeX Font Info: Redefining math symbol \boxtimes on input line 46.
 LaTeX Font Info: Redefining math symbol \blacksquare on input line 48.
 LaTeX Font Info: Redefining math symbol \centerdot on input line 49.
 LaTeX Font Info: Redefining math symbol \blacklozenge on input line 51.

LaTeX Font Info: Redefining math symbol \circlearrowright on input line 52.

LaTeX Font Info: Redefining math symbol \circlearrowleft on input line 53.

LaTeX Font Info: Redefining math symbol \leftrightharpoons on input line 56.

.

LaTeX Font Info: Redefining math symbol \boxminus on input line 57.

LaTeX Font Info: Redefining math symbol \Vdash on input line 58.

LaTeX Font Info: Redefining math symbol \Vvdash on input line 59.

LaTeX Font Info: Redefining math symbol \vDash on input line 60.

LaTeX Font Info: Redefining math symbol \twoheadrightarrow on input line 61.

.

LaTeX Font Info: Redefining math symbol \twoheadleftarrow on input line 62.

LaTeX Font Info: Redefining math symbol \leftleftarrows on input line 63.

LaTeX Font Info: Redefining math symbol \rightrightarrows on input line 64.

LaTeX Font Info: Redefining math symbol \upuparrows on input line 65.

LaTeX Font Info: Redefining math symbol \downdownarrows on input line 66.

LaTeX Font Info: Redefining math symbol \upharpoonright on input line 67.

LaTeX Font Info: Redefining math symbol \downharpoonright on input line 69.

LaTeX Font Info: Redefining math symbol \upharpoonleft on input line 70.

LaTeX Font Info: Redefining math symbol \downharpoonleft on input line 71.

LaTeX Font Info: Redefining math symbol \rightarrowtail on input line 72.

LaTeX Font Info: Redefining math symbol \leftarrowtail on input line 73.

LaTeX Font Info: Redefining math symbol \leftrightarrows on input line 74.

LaTeX Font Info: Redefining math symbol \rightleftarrows on input line 75.

LaTeX Font Info: Redefining math symbol \Lsh on input line 76.

LaTeX Font Info: Redefining math symbol \Rsh on input line 77.

LaTeX Font Info: Redefining math symbol \leftrightsquigarrow on input line 79.

LaTeX Font Info: Redefining math symbol \looparrowleft on input line 80.

LaTeX Font Info: Redefining math symbol \looparrowright on input line 81.

LaTeX Font Info: Redefining math symbol \circeq on input line 82.

LaTeX Font Info: Redefining math symbol \succsim on input line 83.

LaTeX Font Info: Redefining math symbol \gtrsim on input line 84.
 LaTeX Font Info: Redefining math symbol \gtrapprox on input line 85.
 LaTeX Font Info: Redefining math symbol \multimap on input line 86.
 LaTeX Font Info: Redefining math symbol \therefore on input line 87.
 LaTeX Font Info: Redefining math symbol \because on input line 88.
 LaTeX Font Info: Redefining math symbol \doteqdot on input line 89.
 LaTeX Font Info: Redefining math symbol \triangleq on input line 91.
 LaTeX Font Info: Redefining math symbol \precsim on input line 92.
 LaTeX Font Info: Redefining math symbol \lesssim on input line 93.
 LaTeX Font Info: Redefining math symbol \lessapprox on input line 94.
 LaTeX Font Info: Redefining math symbol \eqslantless on input line 95.
 LaTeX Font Info: Redefining math symbol \eqslantgtr on input line 96.
 LaTeX Font Info: Redefining math symbol \curlyeqprec on input line 97.
 LaTeX Font Info: Redefining math symbol \curlyeqsucc on input line 98.
 LaTeX Font Info: Redefining math symbol \preccurlyeq on input line 99.
 LaTeX Font Info: Redefining math symbol \leqq on input line 100.
 LaTeX Font Info: Redefining math symbol \leqslant on input line 101.
 LaTeX Font Info: Redefining math symbol \lessgtr on input line 102.
 LaTeX Font Info: Redefining math symbol \backprime on input line 103.
 LaTeX Font Info: Redefining math symbol \risingdotseq on input line 104.
 LaTeX Font Info: Redefining math symbol \fallingdotseq on input line 105.
 LaTeX Font Info: Redefining math symbol \succcurlyeq on input line 106.
 LaTeX Font Info: Redefining math symbol \geqq on input line 107.
 LaTeX Font Info: Redefining math symbol \geqslant on input line 108.
 LaTeX Font Info: Redefining math symbol \gtrless on input line 109.
 LaTeX Font Info: Redefining math symbol \bigstar on input line 117.
 LaTeX Font Info: Redefining math symbol \between on input line 118.
 LaTeX Font Info: Redefining math symbol \blacktriangledown on input line 119.
 LaTeX Font Info: Redefining math symbol \blacktriangleright on input line 120.
 LaTeX Font Info: Redefining math symbol \blacktriangleleft on input line 121.
 LaTeX Font Info: Redefining math symbol \vartriangle on input line 122.
 LaTeX Font Info: Redefining math symbol \blacktriangle on input line 123.
 LaTeX Font Info: Redefining math symbol \triangledown on input line 124.
 LaTeX Font Info: Redefining math symbol \eqcirc on input line 125.
 LaTeX Font Info: Redefining math symbol \lesseqgtr on input line 126.
 LaTeX Font Info: Redefining math symbol \gtreqless on input line 127.
 LaTeX Font Info: Redefining math symbol \lesseqgtr on input line 128.

LaTeX Font Info: Redefining math symbol \gtreqless on input line 129.
 LaTeX Font Info: Redefining math symbol \Rrightarrow on input line 130.
 LaTeX Font Info: Redefining math symbol \Lleftarrow on input line 131.
 LaTeX Font Info: Redefining math symbol \veebar on input line 132.
 LaTeX Font Info: Redefining math symbol \barwedge on input line 133.
 LaTeX Font Info: Redefining math symbol \doublebarwedge on input line 134.
 LaTeX Font Info: Redefining math symbol \measuredangle on input line 137.
 LaTeX Font Info: Redefining math symbol \sphericalangle on input line 138.
 LaTeX Font Info: Redefining math symbol \varpropto on input line 139.
 LaTeX Font Info: Redefining math symbol \smallsmile on input line 140.
 LaTeX Font Info: Redefining math symbol \smallfrown on input line 141.
 LaTeX Font Info: Redefining math symbol \Subset on input line 142.
 LaTeX Font Info: Redefining math symbol \Supset on input line 143.
 LaTeX Font Info: Redefining math symbol \Cup on input line 144.
 LaTeX Font Info: Redefining math symbol \Cap on input line 146.
 LaTeX Font Info: Redefining math symbol \curlywedge on input line 148.
 LaTeX Font Info: Redefining math symbol \curlyvee on input line 149.
 LaTeX Font Info: Redefining math symbol \leftthreetimes on input line 150.
 LaTeX Font Info: Redefining math symbol \rightthreetimes on input line 151.
 LaTeX Font Info: Redefining math symbol \subseteqq on input line 152.
 LaTeX Font Info: Redefining math symbol \supseteqq on input line 153.
 LaTeX Font Info: Redefining math symbol \bumpeq on input line 154.
 LaTeX Font Info: Redefining math symbol \Bumpeq on input line 155.
 LaTeX Font Info: Redefining math symbol \lll on input line 156.
 LaTeX Font Info: Redefining math symbol \ggg on input line 158.
 LaTeX Font Info: Redefining math symbol \circledS on input line 160.
 LaTeX Font Info: Redefining math symbol \pitchfork on input line 161.
 LaTeX Font Info: Redefining math symbol \dotplus on input line 162.
 LaTeX Font Info: Redefining math symbol \backsim on input line 163.
 LaTeX Font Info: Redefining math symbol \backsimeq on input line 164.
 LaTeX Font Info: Redefining math symbol \complement on input line 165.
 LaTeX Font Info: Redefining math symbol \intercal on input line 166.
 LaTeX Font Info: Redefining math symbol \circledcirc on input line 167.
 LaTeX Font Info: Redefining math symbol \circledast on input line 168.
 LaTeX Font Info: Redefining math symbol \circleddash on input line 169.
 LaTeX Font Info: Redefining math symbol \lvertneqq on input line 171.
 LaTeX Font Info: Redefining math symbol \gvertneqq on input line 172.
 LaTeX Font Info: Redefining math symbol \nleq on input line 173.

LaTeX Font Info: Redefining math symbol \ngeq on input line 174.
 LaTeX Font Info: Redefining math symbol \nless on input line 175.
 LaTeX Font Info: Redefining math symbol \ngtr on input line 176.
 LaTeX Font Info: Redefining math symbol \nprec on input line 177.
 LaTeX Font Info: Redefining math symbol \nsucc on input line 178.
 LaTeX Font Info: Redefining math symbol \lneqq on input line 179.
 LaTeX Font Info: Redefining math symbol \gneqq on input line 180.
 LaTeX Font Info: Redefining math symbol \nleqslant on input line 181.
 LaTeX Font Info: Redefining math symbol \ngeqslant on input line 182.
 LaTeX Font Info: Redefining math symbol \lneq on input line 183.
 LaTeX Font Info: Redefining math symbol \gneq on input line 184.
 LaTeX Font Info: Redefining math symbol \npreceq on input line 185.
 LaTeX Font Info: Redefining math symbol \nsucceq on input line 186.
 LaTeX Font Info: Redefining math symbol \precnsim on input line 187.
 LaTeX Font Info: Redefining math symbol \succnsim on input line 188.
 LaTeX Font Info: Redefining math symbol \lnsim on input line 189.
 LaTeX Font Info: Redefining math symbol \gnsim on input line 190.
 LaTeX Font Info: Redefining math symbol \nleqq on input line 191.
 LaTeX Font Info: Redefining math symbol \ngeqq on input line 192.
 LaTeX Font Info: Redefining math symbol \precneqq on input line 193.
 LaTeX Font Info: Redefining math symbol \succneqq on input line 194.
 LaTeX Font Info: Redefining math symbol \preceqapprox on input line 195.
 LaTeX Font Info: Redefining math symbol \succapprox on input line 196.
 LaTeX Font Info: Redefining math symbol \lnapprox on input line 197.
 LaTeX Font Info: Redefining math symbol \gnapprox on input line 198.
 LaTeX Font Info: Redefining math symbol \nsim on input line 199.
 LaTeX Font Info: Redefining math symbol \ncong on input line 200.
 LaTeX Font Info: Redefining math symbol \diagup on input line 201.
 LaTeX Font Info: Redefining math symbol \diagdown on input line 202.
 LaTeX Font Info: Redefining math symbol \varsubsetneq on input line 203.
 LaTeX Font Info: Redefining math symbol \varsupsetneq on input line 204.
 LaTeX Font Info: Redefining math symbol \nsubseteqq on input line 205.
 LaTeX Font Info: Redefining math symbol \nsupseteqq on input line 206.
 LaTeX Font Info: Redefining math symbol \subsetneqq on input line 207.
 LaTeX Font Info: Redefining math symbol \supsetneqq on input line 208.
 LaTeX Font Info: Redefining math symbol \varsubsetneqq on input line 209.
 LaTeX Font Info: Redefining math symbol \varsupsetneqq on input line 210.
 LaTeX Font Info: Redefining math symbol \subsetneq on input line 211.
 LaTeX Font Info: Redefining math symbol \supsetneq on input line 212.
 LaTeX Font Info: Redefining math symbol \nsubseteq on input line 213.
 LaTeX Font Info: Redefining math symbol \nsupseteq on input line 214.
 LaTeX Font Info: Redefining math symbol \nparallel on input line 215.
 LaTeX Font Info: Redefining math symbol \nmid on input line 216.
 LaTeX Font Info: Redefining math symbol \nshortmid on input line 217.

1
2
3
4
5
6
7
8
9
10
11
12
13
14
15
16
17
18
19
20
21
22
23
24
25
26
27
28
29
30
31
32
33
34
35
36
37
38
39
40
41
42
43
44
45
46
47
48
49
50
51
52
53
54
55
56
57
58
59
60
61
62
63
64
65

LaTeX Font Info:	Redeclaring math symbol \nshortparallel on input line 218.
LaTeX Font Info:	Redeclaring math symbol \nvdash on input line 219.
LaTeX Font Info:	Redeclaring math symbol \nVdash on input line 220.
LaTeX Font Info:	Redeclaring math symbol \nvDash on input line 221.
LaTeX Font Info:	Redeclaring math symbol \nVDash on input line 222.
LaTeX Font Info:	Redeclaring math symbol \ntrianglerighteq on input line 223
.	
LaTeX Font Info:	Redeclaring math symbol \ntrianglelefteq on input line 224.
LaTeX Font Info:	Redeclaring math symbol \ntriangleleft on input line 225.
LaTeX Font Info:	Redeclaring math symbol \ntriangleright on input line 226.
LaTeX Font Info:	Redeclaring math symbol \nleftarrow on input line 227.
LaTeX Font Info:	Redeclaring math symbol \nrightarrow on input line 228.
LaTeX Font Info:	Redeclaring math symbol \nLeftarrow on input line 229.
LaTeX Font Info:	Redeclaring math symbol \nRightarrow on input line 230.
LaTeX Font Info:	Redeclaring math symbol \nLeftrightarrow on input line 231.
LaTeX Font Info:	Redeclaring math symbol \nleqtrightharpoonon input line 232.
LaTeX Font Info:	Redeclaring math symbol \divideontimes on input line 233.
LaTeX Font Info:	Redeclaring math symbol \varnothing on input line 234.
LaTeX Font Info:	Redeclaring math symbol \nexists on input line 235.
LaTeX Font Info:	Redeclaring math symbol \Finv on input line 236.
LaTeX Font Info:	Redeclaring math symbol \Game on input line 237.
LaTeX Font Info:	Redeclaring math symbol \eth on input line 240.
LaTeX Font Info:	Redeclaring math symbol \eqsim on input line 241.
LaTeX Font Info:	Redeclaring math symbol \beth on input line 242.
LaTeX Font Info:	Redeclaring math symbol \gimel on input line 243.
LaTeX Font Info:	Redeclaring math symbol \daleth on input line 244.
LaTeX Font Info:	Redeclaring math symbol \lessdot on input line 245.
LaTeX Font Info:	Redeclaring math symbol \gtrdot on input line 246.
LaTeX Font Info:	Redeclaring math symbol \ltimes on input line 247.
LaTeX Font Info:	Redeclaring math symbol \rtimes on input line 248.
LaTeX Font Info:	Redeclaring math symbol \shortmid on input line 249.
LaTeX Font Info:	Redeclaring math symbol \shortparallel on input line 250.
LaTeX Font Info:	Redeclaring math symbol \smallsetminus on input line 251.
LaTeX Font Info:	Redeclaring math symbol \thicksim on input line 252.
LaTeX Font Info:	Redeclaring math symbol \thickapprox on input line 253.

```

LaTeX Font Info: Redefining math symbol \approx on input line 254.
LaTeX Font Info: Redefining math symbol \succapprox on input line
255.
LaTeX Font Info: Redefining math symbol \precapprox on input line
256.
LaTeX Font Info: Redefining math symbol \curvearrowleft on input line
257.
LaTeX Font Info: Redefining math symbol \curvearrowright on input
line 258.

LaTeX Font Info: Redefining math symbol \digamma on input line 259.
LaTeX Font Info: Redefining math symbol \varkappa on input line 260.
LaTeX Font Info: Redefining math symbol \Bbbk on input line 261.
LaTeX Font Info: Redefining math symbol \hslash on input line 262.
LaTeX Font Info: Redefining math symbol \backepsilon on input line
265.
) (c:/TeXLive/2022/texmf-dist/tex/latex/lineno/lineno.sty
Package: lineno 2023/01/19 line numbers on paragraphs v5.1
\linenopenalty=\count287
\output=\toks31
\linenoprevgraf=\count288
\linenumbersep=\dimen171
\linenumberwidth=\dimen172
\c@linenumber=\count289
\c@pagewiselinenumber=\count290
\c@LN@truepage=\count291
\c@internallinenumber=\count292
\c@internallinenumbers=\count293
\quotelinenumbersep=\dimen173
\bframerule=\dimen174
\bframesep=\dimen175
\bframebox=\box70
\linenoamsmath@ams@eqpen=\count294
LaTeX Info: Redefining \ on input line 3131.
) (c:/TeXLive/2022/texmf-dist/tex/latex/graphics/rotating.sty
Package: rotating 2016/08/11 v2.16d rotated objects in LaTeX
(c:/TeXLive/2022/texmf-dist/tex/latex/base/ifthen.sty
Package: ifthen 2022/04/13 v1.1d Standard LaTeX ifthen package (DPC)
)
\c@r@tfl@t=\count295
\rotFPtop=\skip62
\rotFPbot=\skip63
\rot@float@box=\box71
\rot@mess@toks=\toks32
) (c:/TeXLive/2022/texmf-dist/tex/generic/soul/soul.sty
Package: soul 2023-02-18 v3.0 Permit use of UTF-8 characters in soul (HO)
(c:/TeXLive/2022/texmf-dist/tex/generic/soul/soul-ori.sty
Package: soul-ori 2023-02-18 v3.0 letterspacing/underlining (mf)
\SOUL@word=\toks33
\SOUL@lasttoken=\toks34
\SOUL@syllable=\toks35
\SOUL@cmds=\toks36
\SOUL@buffer=\toks37
\SOUL@token=\toks38

```



```

1
2
3
4 \SOUL@syllgoal=\dimen176
5 \SOUL@syllwidth=\dimen177
6 \SOUL@charkern=\dimen178
7 \SOUL@hyphkern=\dimen179
8 \SOUL@dimen=\dimen180
9 \SOUL@dimeni=\dimen181
10 \SOUL@minus=\count296
11 \SOUL@comma=\count297
12 \SOUL@apo=\count298
13 \SOUL@grave=\count299
14 \SOUL@spaceskip=\skip64
15 \SOUL@ttwidth=\dimen182
16 \SOUL@uldp=\dimen183
17 \SOUL@ulht=\dimen184
18 ) (c:/TeXLive/2022/texmf-dist/tex/generic/infwarerr/infwarerr.sty
19 Package: infwarerr 2019/12/03 v1.5 Providing info/warning/error messages
20 (HO)
21 ) (c:/TeXLive/2022/texmf-dist/tex/generic/etexcmds/etexcmds.sty
22 Package: etexcmds 2019/12/15 v1.7 Avoid name clashes with e-TeX commands
23 (HO)
24 )) (c:/TeXLive/texmf-local/tex/latex/aries/subfigure.sty
25 Package: subfigure 2002/03/15 v2.1.5 subfigure package
26 \subfigtopskip=\skip65
27 \subfigcapskip=\skip66
28 \subfigcaptopadj=\dimen185
29 \subfigbottomskip=\skip67
30 \subfigcapmargin=\dimen186
31 \subfiglabelskip=\skip68
32 \c@subfigure=\count300
33 \c@lofdepth=\count301
34 \c@subtable=\count302
35 \c@lotdepth=\count303
36 *****
37 * Local config file subfigure.cfg used *
38 *****
39 (c:/TeXLive/texmf-local/tex/latex/aries/subfigure.cfg)
40 \subfig@top=\skip69
41 \subfig@bottom=\skip70
42 ) (./main_scripta_rev.aux)
43 \openout1 = `main_scripta_rev.aux'.
44
45
46
47 LaTeX Font Info: Checking defaults for OML/txmi/m/it on input line 57.
48 LaTeX Font Info: Trying to load font information for OML+txmi on input
49 line
50 57.
51 (c:/TeXLive/2022/texmf-dist/tex/latex/txfonts/omltxmi.fd
52 File: omltxmi.fd 2000/12/15 v3.1
53 )
54 LaTeX Font Info: ... okay on input line 57.
55 LaTeX Font Info: Checking defaults for OMS/txsy/m/n on input line 57.
56 LaTeX Font Info: Trying to load font information for OMS+txsy on input
57 line
58 57.
59 (c:/TeXLive/2022/texmf-dist/tex/latex/txfonts/omstxsy.fd
60
61
62
63
64
65

```

```

1
2
3
4 File: omstxsy.fd 2000/12/15 v3.1
5 )
6 LaTeX Font Info:    ... okay on input line 57.
7 LaTeX Font Info:    Checking defaults for OT1/cmr/m/n on input line 57.
8 LaTeX Font Info:    ... okay on input line 57.
9 LaTeX Font Info:    Checking defaults for T1/cmr/m/n on input line 57.
10 LaTeX Font Info:    ... okay on input line 57.
11 LaTeX Font Info:    Checking defaults for TS1/cmr/m/n on input line 57.
12 LaTeX Font Info:    ... okay on input line 57.
13 LaTeX Font Info:    Checking defaults for OMX/txex/m/n on input line 57.
14 LaTeX Font Info:    Trying to load font information for OMX+txex on input
15 line
16 57.
17 (c:/TeXLive/2022/texmf-dist/tex/latex/txfonts/omctxex.fd
18 File: omctxex.fd 2000/12/15 v3.1
19 )
20 LaTeX Font Info:    ... okay on input line 57.
21 LaTeX Font Info:    Checking defaults for U/txexa/m/n on input line 57.
22 LaTeX Font Info:    Trying to load font information for U+txexa on input
23 line 5
24 7.
25 (c:/TeXLive/2022/texmf-dist/tex/latex/txfonts/utxexa.fd
26 File: utxexa.fd 2000/12/15 v3.1
27 )
28 LaTeX Font Info:    ... okay on input line 57.
29 (c:/TeXLive/2022/texmf-dist/tex/context/base/mkii/supp-pdf.mkii
30 [Loading MPS to PDF converter (version 2006.09.02).]
31 \scratchcounter=\count304
32 \scratchdimen=\dimen187
33 \scratchbox=\box72
34 \nofMPsegments=\count305
35 \nofMParguments=\count306
36 \everyMPshowfont=\toks39
37 \MPscratchCnt=\count307
38 \MPscratchDim=\dimen188
39 \MPnumerator=\count308
40 \makeMPintoPDFobject=\count309
41 \everyMPtoPDFconversion=\toks40
42 ) (c:/TeXLive/2022/texmf-dist/tex/latex/epstopdf-pkg/epstopdf-base.sty
43 Package: epstopdf-base 2020-01-24 v2.11 Base part for package epstopdf
44 Package epstopdf-base Info: Redefining graphics rule for '.eps' on input
45 line 4
46 85.
47 (c:/TeXLive/2022/texmf-dist/tex/latex/latexconfig/epstopdf-sys.cfg
48 File: epstopdf-sys.cfg 2010/07/13 v1.3 Configuration of (r)epstopdf for
49 TeX Liv
50 e
51 ))
52 *geometry* driver: auto-detecting
53 *geometry* detected driver: pdftex
54 *geometry* verbose mode - [ preamble ] result:
55 * driver: pdftex
56 * paper: custom
57 * layout: <same size as paper>
58
59
60
61
62
63
64
65

```

```

* layoutoffset: (h,v)=(0.0pt,0.0pt)
* hratio: 1:1
* vratio: 1:1
* modes:
* h-part: (L,W,R)=(37.75394pt, 522.0pt, 37.75394pt)
* v-part: (T,H,B)=(81.52342pt, 682.0pt, 81.52342pt)
* \paperwidth=597.50787pt
* \paperheight=845.04684pt
* \textwidth=522.0pt
* \textheight=682.0pt
* \oddsidemargin=-34.51605pt
* \evensidemargin=-34.51605pt
* \topmargin=-52.74657pt
* \headheight=50.0pt
* \headsep=12.0pt
* \topskip=10.0pt
* \footskip=18.0pt
* \marginparwidth=65.0pt
* \marginparsep=11.0pt
* \columnsep=18.0pt
* \skip\footins=24.0pt plus 2.0pt minus 12.0pt
* \hoffset=0.0pt
* \voffset=0.0pt
* \mag=1000
* \@twocolumntrue
* \@twosidefalse
* \@mparswitchfalse
* \@reversemarginfalse
* (lin=72.27pt=25.4mm, 1cm=28.453pt)

```

```

\symgns@font=\mathgroup11

```

```

LaTeX Font Info: Overwriting symbol font `gns@font' in version `bold'
(Font) TS1/lmr/m/n --> TS1/lmr/b/n on input line 57.

```

```

Package gensymb Info: Math companion symbols declared on input line 57.

```

```

LaTeX Info: Redefining \degree on input line 57.

```

```

LaTeX Info: Redefining \celsius on input line 57.

```

```

Package gensymb Info: Using text companion symbols for \degree, \celsius
and \p

```

```

erthousand on input line 57.

```

```

LaTeX Info: Redefining \ohm on input line 57.

```

```

Package gensymb Info: Using \textohm for \ohm on input line 57.

```

```

Package gensymb Info: Using \textmu for \micro on input line 57.

```

```

LaTeX Font Info: Trying to load font information for OT1+lmr on input
line 1

```

```

00.

```

```

(c:/TeXLive/2022/texmf-dist/tex/latex/lm/ot1lmr.fd

```

```

File: ot1lmr.fd 2015/05/01 v1.6.1 Font defs for Latin Modern

```

```

)

```

```

LaTeX Font Info: Trying to load font information for OML+lmm on input
line 1

```

```

00.

```

```

(c:/TeXLive/2022/texmf-dist/tex/latex/lm/oml1lmm.fd

```

```

File: oml1lmm.fd 2015/05/01 v1.6.1 Font defs for Latin Modern

```

```

)

```



```
1
2
3
4 LaTeX Font Info: Trying to load font information for OMS+lmsy on input
5 line
6 100.
7 (c:/TeXLive/2022/texmf-dist/tex/latex/lm/omslmsy.fd
8 File: omslmsy.fd 2015/05/01 v1.6.1 Font defs for Latin Modern
9 )
10 LaTeX Font Info: Trying to load font information for OMX+lmex on input
11 line
12 100.
13 (c:/TeXLive/2022/texmf-dist/tex/latex/lm/omxlmex.fd
14 File: omxlmex.fd 2015/05/01 v1.6.1 Font defs for Latin Modern
15 )
16 LaTeX Font Info: External font `lmex10' loaded for size
17 (Font) <10> on input line 100.
18 LaTeX Font Info: External font `lmex10' loaded for size
19 (Font) <7> on input line 100.
20 LaTeX Font Info: External font `lmex10' loaded for size
21 (Font) <5> on input line 100.
22 LaTeX Font Info: Trying to load font information for OTl+txr on input
23 line 1
24 00.
25 (c:/TeXLive/2022/texmf-dist/tex/latex/txfonts/otltxr.fd
26 File: otltxr.fd 2000/12/15 v3.1
27 )
28 LaTeX Font Info: Trying to load font information for U+txmia on input
29 line 1
30 00.
31 (c:/TeXLive/2022/texmf-dist/tex/latex/txfonts/utxmia.fd
32 File: utxmia.fd 2000/12/15 v3.1
33 )
34 LaTeX Font Info: Trying to load font information for U+msa on input
35 line 100
36 .
37 (c:/TeXLive/2022/texmf-dist/tex/latex/amsfonts/umsa.fd
38 File: umsa.fd 2013/01/14 v3.01 AMS symbols A
39 )
40 LaTeX Font Info: Trying to load font information for U+msb on input
41 line 100
42 .
43 (c:/TeXLive/2022/texmf-dist/tex/latex/amsfonts/umsb.fd
44 File: umsb.fd 2013/01/14 v3.01 AMS symbols B
45 )
46 LaTeX Font Info: Trying to load font information for U+txsyc on input
47 line 1
48 00.
49 (c:/TeXLive/2022/texmf-dist/tex/latex/txfonts/utxsyc.fd
50 File: utxsyc.fd 2000/12/15 v3.1
51 )
52 LaTeX Font Info: Trying to load font information for TS1+lmr on input
53 line 1
54 00.
55 (c:/TeXLive/2022/texmf-dist/tex/latex/lm/ts1lmr.fd
56 File: ts1lmr.fd 2015/05/01 v1.6.1 Font defs for Latin Modern
57 )
58
59
60
61
62
63
64
65
```

LaTeX Font Info: External font `lmex10' loaded for size
(Font) <8> on input line 115.
LaTeX Font Info: External font `lmex10' loaded for size
(Font) <6> on input line 115.
LaTeX Font Info: Trying to load font information for T1+lmmtt on input
line 1
15.
(c:/TeXLive/2022/texmf-dist/tex/latex/lm/t1lmtt.fd
File: t1lmtt.fd 2015/05/01 v1.6.1 Font defs for Latin Modern
)

Package natbib Warning: Citation `gu2012laser' on page 1 undefined on
input line 118.

Package natbib Warning: Citation `hooper2018melt' on page 1 undefined on
input line 119.

Package natbib Warning: Citation `fergani2017' on page 1 undefined on
input line 119.

Package natbib Warning: Citation `li2018residual' on page 1 undefined on
input line 119.

Package natbib Warning: Citation `WANG201768' on page 1 undefined on
input line 121.

Package natbib Warning: Citation `GOKCEKAYA2020101624' on page 1
undefined on input line 121.

Package natbib Warning: Citation `ALAM2020110138' on page 1 undefined on
input line 121.

Package natbib Warning: Citation `honnige2017improvement' on page 1
undefined on input line 121.

Package natbib Warning: Citation `zhao2017real' on page 1 undefined on
input line 123.

Package natbib Warning: Citation `leung2018situ' on page 1 undefined on input line 123.

Package natbib Warning: Citation `chen2021synchrotron' on page 1 undefined on input line 123.

Package natbib Warning: Citation `thompson2016x' on page 1 undefined on input line 123.

Package natbib Warning: Citation `wolff2021situ' on page 1 undefined on input line 123.

Package natbib Warning: Citation `prithivirajan2021direct' on page 1 undefined on input line 123.

Package natbib Warning: Citation `ludwig2008x' on page 1 undefined on input line 123.

Overfull \hbox (2.22221pt too wide) has occurred while \output is active
[]
[]

[1{c:/TeXLive/2022/texmf-var/fonts/map/pdftex/updmap/pdftex.map}]

Package natbib Warning: Citation `Simons2015' on page 2 undefined on input line 125.

Package natbib Warning: Citation `yildirim2020probing' on page 2 undefined on input line 125.

LaTeX Warning: File `figures/EBSD_DF_BuildDirection.png' not found on input line 135.

1
2
3
4
5
6 ! Package pdftex.def Error: File `figures/EBSD_DF_BuildDirection.png' not
7 found
8 : using draft setting.
9

10 See the pdftex.def package documentation for explanation.
11 Type H <return> for immediate help.
12 ...
13

14 1.135 ...hics{figures/EBSD_DF_BuildDirection.png}}

15
16 Try typing <return> to proceed.
17 If that doesn't work, type X <return> to quit.
18
19
20

21 LaTeX Warning: `!h' float specifier changed to `!ht'.
22
23

24 LaTeX Warning: File `figures/Fig2_BuildDirection.png' not found on input
25 line 1
26 44.
27
28

29 ! Package pdftex.def Error: File `figures/Fig2_BuildDirection.png' not
30 found: u
31 sing draft setting.
32

33 See the pdftex.def package documentation for explanation.
34 Type H <return> for immediate help.
35 ...
36

37 1.144 ...raphics{figures/Fig2_BuildDirection.png}}

38
39 Try typing <return> to proceed.
40 If that doesn't work, type X <return> to quit.
41
42
43

44 LaTeX Warning: `h' float specifier changed to `ht'.
45
46

47 Package natbib Warning: Citation `tang2020effect' on page 2 undefined on
48 input
49 line 151.
50
51

52 Package natbib Warning: Citation `WILKINSON2012366' on page 2 undefined
53 on input
54 line 155.
55
56

57 Package natbib Warning: Citation `Britton2013' on page 2 undefined on
58 input line
59 155.
60
61
62
63
64
65

Package natbib Warning: Citation `WMG2006_1' on page 2 undefined on input line 155.

Package natbib Warning: Citation `WILKINSON2006307' on page 2 undefined on input line 155.

Package natbib Warning: Citation `Kutsal2019' on page 2 undefined on input line 158.

Package natbib Warning: Citation `darfix' on page 2 undefined on input line 159

.

[2]

Package natbib Warning: Citation `yildirim20224d' on page 3 undefined on input line 164.

Package natbib Warning: Citation `yildirim2022multiscale' on page 3 undefined on input line 164.

Package natbib Warning: Citation `darfix' on page 3 undefined on input line 164

.

LaTeX Warning: File `figures/com_misor_2.png' not found on input line 170.

! Package pdftex.def Error: File `figures/com_misor_2.png' not found: using default setting.

See the pdftex.def package documentation for explanation.
Type H <return> for immediate help.
...

1.170 ...includegraphics{figures/com_misor_2.png}}

Try typing <return> to proceed.
If that doesn't work, type X <return> to quit.

LaTeX Warning: File `figures/2x_mosaicity_3d_layers.png' not found on input line 181.

! Package pdftex.def Error: File `figures/2x_mosaicity_3d_layers.png' not found
: using draft setting.

See the pdftex.def package documentation for explanation.
Type H <return> for immediate help.

...

l.181 ...hics{figures/2x_mosaicity_3d_layers.png}}

Try typing <return> to proceed.
If that doesn't work, type X <return> to quit.

Package natbib Warning: Citation `raabe' on page 3 undefined on input line 186.

Package natbib Warning: Citation `tang2023multi' on page 3 undefined on input line 186.

Package natbib Warning: Citation `yildirim20224d' on page 3 undefined on input line 188.

Package natbib Warning: Citation `mavrikakis2019' on page 3 undefined on input line 188.

Package natbib Warning: Citation `KONTIS201876' on page 3 undefined on input line 188.

Package natbib Warning: Citation `munoz2016effect' on page 3 undefined on input line 188.

Package natbib Warning: Citation `tang2023multi' on page 3 undefined on input line 188.

Package natbib Warning: Citation `hlushko2020dark' on page 3 undefined on input line 192.

Package natbib Warning: Citation `tang2023multi' on page 3 undefined on input line 194.

Package natbib Warning: Citation `aba2016determination' on page 3 undefined on input line 194.

Package natbib Warning: Citation `tang2020effect' on page 3 undefined on input line 194.

[3]

Package natbib Warning: Citation `TANG2021116468' on page 4 undefined on input line 196.

Package natbib Warning: Citation `debroy2018additive' on page 4 undefined on input line 198.

Package natbib Warning: Citation `jahangiri2012study' on page 4 undefined on input line 198.

Package natbib Warning: Citation `tang2023multi' on page 4 undefined on input line 198.

LaTeX Warning: File `figures/Fig5_PostReview.png' not found on input line 203.

! Package pdftex.def Error: File `figures/Fig5_PostReview.png' not found: using draft setting.

See the pdftex.def package documentation for explanation.
Type H <return> for immediate help.

...

1.203 ...udegraphics{figures/Fig5_PostReview.png}}

Try typing <return> to proceed.

If that doesn't work, type X <return> to quit.

LaTeX Warning: `!h' float specifier changed to `!ht'.

Package natbib Warning: Citation `tang2023multi' on page 4 undefined on
input 1
ine 210.

[4]
No file main_scripta_rev.bbl.

Package natbib Warning: There were undefined citations.

- LAST -
Extra skip:682.0pt
Left:682.0pt/0.0pt
Right:0.0pt/0.0pt
Split: 341.0pt
Output:341.0pt
Pageshrink: 0.0pt
Pagestretch: 0.0pt
@colht:682.0pt
FLUSHEND [output]: 341.0pt
FLUSHEND [leftcolumn badness]: 1000000
FUSHEND [rightcolumn badness]: 0
[5] [6] [7]

] [8] [9]

] (./main_scripta_rev.aux))

Here is how much of TeX's memory you used:

7516 strings out of 476024
114696 string characters out of 5794017
1876382 words of memory out of 5000000
27754 multiletter control sequences out of 15000+600000
576943 words of font info for 101 fonts, out of 8000000 for 9000
1141 hyphenation exceptions out of 8191
72i,9n,76p,2417b,305s stack positions out of
10000i,1000n,20000p,200000b,200000s
{c:/TeXLive/2022/texmf-dist/fonts/enc/dvips/lm/lm-r
m.enc}{c:/TeXLive/2022/texmf-dist/fonts/enc/dvips/lm/lm-
tsl.enc}{c:/TeXLive/202
2/texmf-dist/fonts/enc/dvips/lm/lm-mathit.enc}{c:/TeXLive/2022/texmf-
dist/fonts
/enc/dvips/lm/lm-mathex.enc}{c:/TeXLive/2022/texmf-
dist/fonts/enc/dvips/lm/lm-m

1
2
3
4 athsy.enc}{c:/TeXLive/2022/texmf-dist/fonts/enc/dvips/lm/lm-
5 ec.enc}<c:/TeXLive/
6 2022/texmf-
7 dist/fonts/type1/public/amsfonts/euler/eurm10.pfb><c:/TeXLive/2022/t
8 exmf-dist/fonts/type1/public/lm/lmbx10.pfb><c:/TeXLive/2022/texmf-
9 dist/fonts/ty
10 pel/public/lm/lmex10.pfb><c:/TeXLive/2022/texmf-
11 dist/fonts/type1/public/lm/lmmi
12 10.pfb><c:/TeXLive/2022/texmf-
13 dist/fonts/type1/public/lm/lmmi8.pfb><c:/TeXLive/
14 2022/texmf-dist/fonts/type1/public/lm/lmr10.pfb><c:/TeXLive/2022/texmf-
15 dist/fon
16 ts/type1/public/lm/lmr12.pfb><c:/TeXLive/2022/texmf-
17 dist/fonts/type1/public/lm/
18 lmr6.pfb><c:/TeXLive/2022/texmf-
19 dist/fonts/type1/public/lm/lmr7.pfb><c:/TeXLive
20 /2022/texmf-dist/fonts/type1/public/lm/lmr8.pfb><c:/TeXLive/2022/texmf-
21 dist/fon
22 ts/type1/public/lm/lmri10.pfb><c:/TeXLive/2022/texmf-
23 dist/fonts/type1/public/lm
24 /lmri7.pfb><c:/TeXLive/2022/texmf-
25 dist/fonts/type1/public/lm/lmri8.pfb><c:/TeXL
26 ive/2022/texmf-
27 dist/fonts/type1/public/lm/lmsy10.pfb><c:/TeXLive/2022/texmf-dis
28 t/fonts/type1/public/lm/lmsy6.pfb><c:/TeXLive/2022/texmf-
29 dist/fonts/type1/publi
30 c/lm/lmsy7.pfb><c:/TeXLive/2022/texmf-
31 dist/fonts/type1/public/lm/lmsy8.pfb><c:/
32 TeXLive/2022/texmf-
33 dist/fonts/type1/public/lm/lmtt10.pfb><c:/TeXLive/2022/texmf
34 -dist/fonts/type1/public/lm/lmtt8.pfb>
35 Output written on main_scripta_rev.pdf (9 pages, 332619 bytes).
36 PDF statistics:
37 150 PDF objects out of 1000 (max. 8388607)
38 95 compressed objects within 1 object stream
39 0 named destinations out of 1000 (max. 500000)
40 1 words of extra memory for PDF output out of 10000 (max. 10000000)
41
42
43
44
45
46
47
48
49
50
51
52
53
54
55
56
57
58
59
60
61
62
63
64
65



[Click here to access/download](#)

LaTeX Source Files
ref_test.bib

